DRAFT

A MATHEMATICAL MODEL OF AIRCRAFT CARGO COMPARTMENT FIRES

Charles D. MacArthur

David J. Grove

University of Dayton
Research Institute
Dayton, Ohio

January 1984

DRAFT

Prepared for

U.S. Department of Transportation
Federal Aviation Administration
Technical Center
Atlantic City Airport, NJ 08405

PREFACE

This report was prepared by the University of Dayton Research Institute for the Federal Aviation Administration Technical Center under Contract DTFA03-C-82-00022 during the period 12 March 1982 through 30 April 1983. Richard Hill and David Blake served as contract technical officers.

Work was performed at the university under the supervision of Nicholas A. Engler and James K. Luers. Programming assistance was provided by Zalfa Challita. Stevie Ann Hardyal edited the document and Gretchen Walther, Lynn Nash, and Nahla Abdelnour prepared the typescript. The authors wish to thank all those mentioned for their valuable suggestions, patience, and encouragement.

This report is dedicated to the memory of Dr. Richard B. Wallace, Lt. Col. USAF Ret., our respected colleague who perished in a fire in his home December 31, 1981.

NOMENCLATURE

Symbol	Definition	Units
A	Area	m^2
b	Fire (flame or plume) column radius	m
C	A constant in Equation (18)	-
c	Specific heat	J/kg-K
D	Distance from fire base to zone interface	m
d	Flame length, distance along flame axis	m
E_c	Combustion efficiency	-
F	Radiation view factor	-
f	Function defined in Equation (33)	J/kg
G	Mass flow	kg/s
Gr	Grashof number	-
g	Gravitational acceleration	m/s^2
H	Distance from fire base to ceiling	m
h	Convective heat transfer coefficient	W/m^2-K
I	Enthalpy, also	J
I	Integral and analytic approximation used in Equation (33)	
$\dot{I}$	Enthalpy flow	J/s
J	Fraction of theoretical heat of combustion that results in fire gas temperature rise	-
K	Entrainment coefficient	-
$\bar{k}$	Absorption coefficient	m^{-1}
k	Thermal conductivity	W/m-K
L	Heat of vaporization, also	J/kg
L	Panel length scale, also	m
L	Mean beam length	m
ℓ	Mean beam length	m
M	Mass	kg
$\dot{m}''$	Mass flux	kg/m^2-s
Nu	Nusselt number	-

n	Surface normal vector or component (magnitude)	-
P	Pressure	Pa
Pr	Prandtl number	-
$\dot{Q}$	Heat flow	W
$\dot{q}"$	Heat flux	W/m^2
R	Gas constant	J/kg-K
$\bar{R}$	Universal gas constant	J/kgmole-K
Re	Reynolds number	-
r	Stoichiometric ratio, also	-
r	Distance	m
s	Material thickness	m
T	Temperature	K
t	Time	s
U	Distance	m
u	Velocity	m/s
V	Volume	m^3
$\dot{V}$	Volume flow rate	m^3/s
W	Term defined by Equation (36)	-
x	Coordinate	m
Y	Species mass fraction	-
y	Coordinate	m
Z	Zone thickness	m
z	Coordinate	m

GREEK

α	Variable of integration	-
β	Variable of integration	-
γ	Term defined in Equation (34)	-
ΔH_c	Heat of combustion	J/kg
ε	Emittance	-
ζ	Mass flow ratio in cool zone	-
η	Mass flow ratio in hot zone	-
θ	Angle	-

λ	Wave length	m
ν	Stoichiometric coefficient, also	-
ν	Kinematic viscosity	m^2/s
ρ	Density	kg/m^3
σ	Stefan-Boltzmann constant	W/m^2-K^4
Φ	Angle	-
χ_r	Radiated fraction	-
ψ	Variable of integration	-
ω	Molecular weight	kg/kgmole

SUBSCRIPTS

amb	Ambient conditions
b	Flame base
c	Cool zone
ce	convection on exterior
ci	convection on interior
CO_2	Carbon dioxide
ext	Exterior
f	Fire, fuel, flame
fc	To fire from cool zone
fi	Fuel at zone interface
fh	To fire from hot zone
fo	Fuel at flame base
g	Gasification
H_2O	Water vapor
h	Hot zone
hf	To hot zone from fire
i	Summation index
j	Species index
N_2	Nitrogen
O_2	Oxygen
p	Plume, pressure (constant)
r	Radiation

re	Radiation at exterior surface
rfb	Radiation incoming at flame base
ri	Radiation at interior surface
rih	Radiation incoming to hot zone
roh	Radiation leaving hot zone
rr	Fuel surface re-radiation
S	Smoke, soot
s	Of wall material
t	Flame tip
vc	Through vents in contact with cool zone
vh	Through vents in contact with hot zone
w	Wall
0 (zero)	Fire base value

SECTION 1
INTRODUCTION

1.1 PURPOSE

This report describes a mathematical model and computer code created to simulate a fire in a cargo compartment of a transport aircraft. The Cargo Compartment Fire Model (CCFM) is intended to provide a means to evaluate the design--in particular, the size, shape, and ventilation--of cargo compartments in relation to their abilities to contain a growing fire.

1.2 BACKGROUND

Fire in a cargo compartment of a transport aircraft presents an obvious extreme danger to the passengers and crew. The necessarily light construction of the compartment walls and ceiling and the location of most compartments in close proximity to the cabin allows little resistance to the penetration of flames, smoke, and gases into the inhabited spaces of the airplane. Since the cargo compartment is an unoccupied space, automatic detectors must be relied upon to sense an incipient fire. For control, or better, extinguishment, two approaches have been taken based upon the compartment volume. If the compartment is sufficiently small the practice is not to provide automatic extinguishment equipment but simply to shut-off all ventilation in the hope that the fire will suffocate. For larger compartments enough oxygen will be present in the larger volume after ventilation shut-off to necessitate an extinguishment system. The question naturally arises as to how large a compartment can be before an extinguishment system is required. To help answer this question and others concerning cargo fires we have constructed a mathematical model of the process.

The model uses the zone method of analysis of enclosed fires. This method has received considerable development in

recent years and is gaining general acceptance as a practical tool. Zone modeling attempts to deal with the many complex physical processes of fires in enclosures by combining simplified, approximate treatments of the more-or-less distinct parts of the problem: the fire itself, the collection of hot gases at the ceiling, the interior radiation, and the fuel heating and gasification. As each part is treated separately, zone models and their computer codes take on a modular structure which facilitates modifications, refinements, and generalizations by replacing individual modules (sub-models) with improved versions. In this sense the CCFM is an outgrowth of earlier zone models, in particular the DACFIR3 model of aircraft cabin fires [Ref. 1], although a completely new computer code was created for the cargo compartment problem. The CCFM differs from other zone models in its emphasis on the effect of reduced oxygen on the fire burning rate. To incorporate this effect newly available treatments of the fire combustion process and heat transfer to the walls and ceiling were adapted for this application.

This report decribes the mathematical development of the model and presents the results for a sample test case. A companion volume comprises the User's Guide for the CCFM code. The model has not yet been compared to the results of physical experiment so that many of the assumptions and approximations described herein await validation. We hope that suitable tests of the model will be available soon.

SECTION 2
THE MATHEMATICAL MODEL

This section presents the mathematical development of the CCFM. Many good expositions of the fundamentals of zone modeling are available, for example, Emmons [Ref. 2], Qunitiere and McCaffrey [Ref. 3], and Mitler [Ref. 4]. The reader should consult these references for a background and further details of the method.

2.1 ZONE MODELING OF ENCLOSED FIRES

Consider the loaded cargo compartment shown in Figure 1. A fire has started and grown to a scale of perhaps one-half meter in base diameter. (The fire base is the burning surface area of the solid or liquid fuel.) Products of combustion, generated at the fire base and in the flames, rise to the upper part of the compartment due to their buoyancy and collect there, heating the compartment walls and ceiling. Flames may impinge on the ceiling and wash over it to involve the walls and other parts of the cargo load. Heat is transferred to the compartment structure by convection and radiation from the hot gas and flames. Given sufficient exposure, the structure may ignite, burn-through, and collapse. Radiation from the hot gases and heated upper parts of the compartment returns energy to the vaporizing fuel surface, creating the typical positive feedback and exponentially accelerating growth of enclosed fires.

The compartment may be ventilated by ducts, as shown, and by leakage (infiltration) from the cabin above. The ventilation mechanism is one of the major differences between the cargo compartment and cabin or room fire situations. For cabin fires the ventilation is most likely to be by buoyant flow out of large openings, that is, doors, during the post-crash evacuation. For cargo compartment fires the primary interest is in the inflight fire where the ventilation may be "forced" (flows driven by the

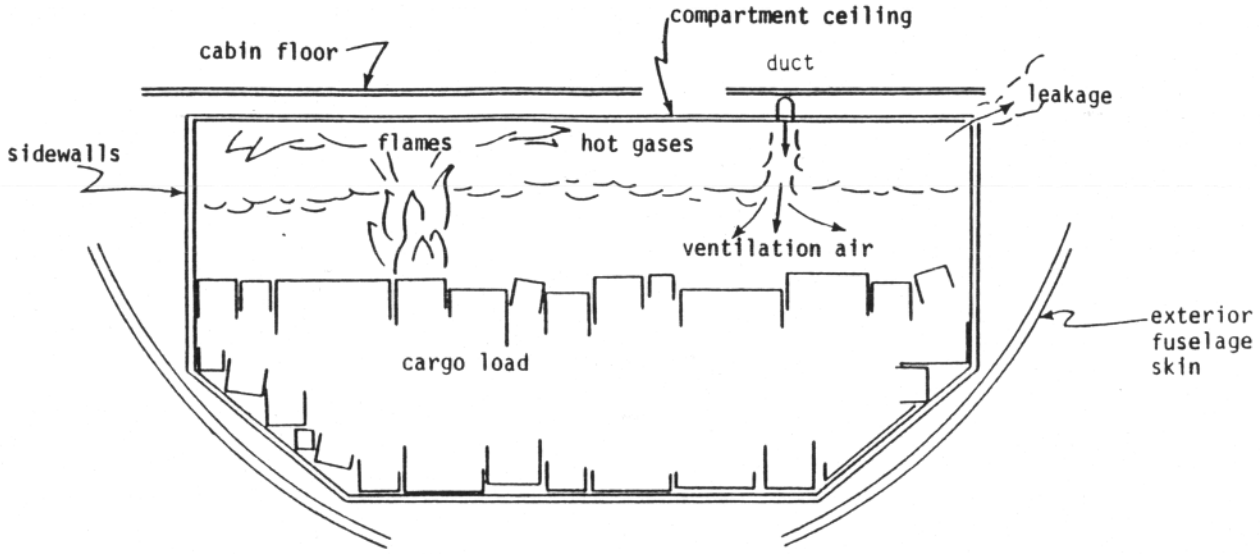

Figure 1. Typical Cargo Compartment Arrangement with a Developing Fire. The Load Could be "Loose Fill" Items Such as Baggage or Palletized Freight.

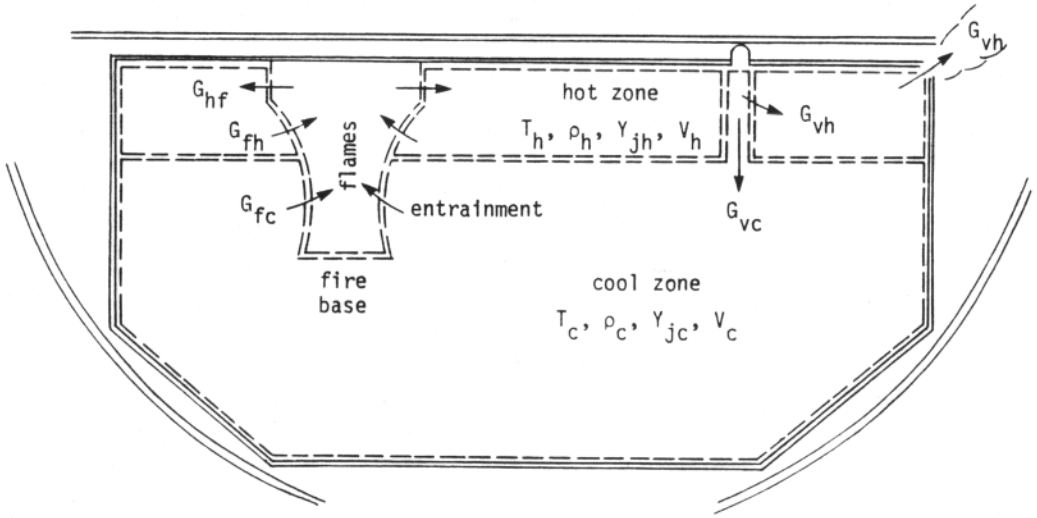

Figure 2. The Compartment Atmosphere is Divided into Hot (Upper) and Cool (Lower) Zones for Analysis. The Major Mass Flows are Fuel Vaporization, Fire Entrainment, Ventilation, and Leakage. Energy Flows are Fire Heat Release, Convective and Radiative Flows to the Walls, etc., Ventilation, and Leakage.

ventilation system) and may also involve small leakage flows caused by the overall rise in internal pressure.

Figure 2 shows how, in the zone method, the interior volume of the compartment is divided into two control volumes or zones: the upper zone consisting of combustion products and heated air, and the lower consisting of the original uncontaminated air which may be augmented by inflow ventilation under the appropriate circumstances.

A basic assumption of zone modeling is that both the upper (hot) and lower (cool) zones are always sufficiently well-mixed so that single values for the temperature, density, and species mass fractions may be used to describe each zone. This assumption has profound importance with respect to the mathematical form of the model. The conservation laws applied to each zone result in a set of ordinary differential equations rather than partial differential equations. Consequently, the task of numerical solution is greatly simplified. The development of the governing equations for each zone is discussed in Section 2.3.

Mixing between the zones across the "thermal discontinuity plane" which separates them is assumed to be totally suppressed by the action of buoyancy. The only way mass can be transferred between the zones is by the entrainment of cool zone air into the fire flame and plume column and the consequent deposition of this gas in the hot zone.

Energy exchanges between the zones, the fire, and their surroundings take several forms. Some of the sensible energy generated in the flames is radiated immediately to the surroundings while another part is transported to the hot zone through the plume. The hot zone radiates energy and heats the surfaces it touches by convection. It will also absorb radiation from the flames and from heated surfaces. Common practice in zone modeling has been to ignore radiation exchanges with the cool

zone gas and we have followed it here, although radiation terms are formally included in the governing equations. The cool zone does gain heat by convection from the heated surfaces it touches, and, by an effect not always included in other models, compressional heating by the expanding hot zone. Similarly, the work done by the hot zone in expanding can serve to lower its energy. These processes and others are discussed in quantitative terms in Section 2.3.

Because the hot and cool zones are separate and unmixed throughout the simulation, the method by which the reduced oxygen in a compartment affects the fire flames is the envelopment of the fire by the hot zone as time passes. Extension of the flame and plume into the hot zone has not been considered in existing zone models, primarily because vitiation effects were not of interest. To account for the effect of the hot zone temperature and composition on the fire we require a model of the flame structure and fuel combustion with more realistic detail than has been used before. Fortunately, a model which meets these requirements has recently become available. We give the details of the flame and plume model in Section 2.6.

2.2 COMPARTMENT DESCRIPTION

The compartment description assumed by the CCFM consists of a closed box made of connected planes. Figure 3 shows a typical shape and the coordinate system used to specify all dimensions and distances. The compartment is located so that all coordinates are greater than or equal to zero in this rectangular x-y-z system. We further assume that the compartment cross-section parallel to the x-z plane is constant with y and convex in shape. The two end walls must be parallel to the x-z plane and, by the previous assumption, they are equal in size and shape.

For the purpose of computing their surface temperatures, the compartment walls, ceiling, and floor may be subdivided into

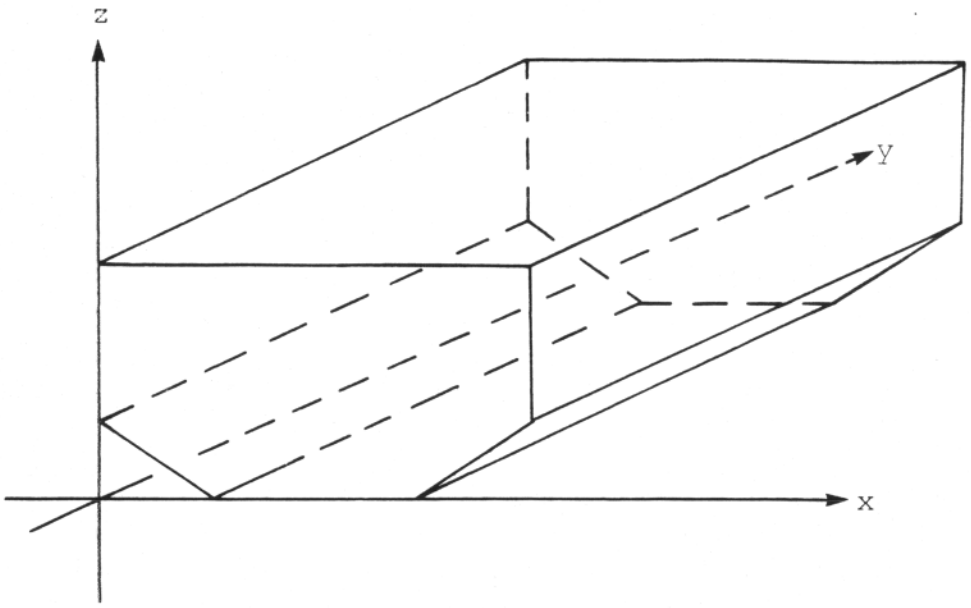

Figure 3. Typical Cargo Compartment Shape and the Coordinate System.

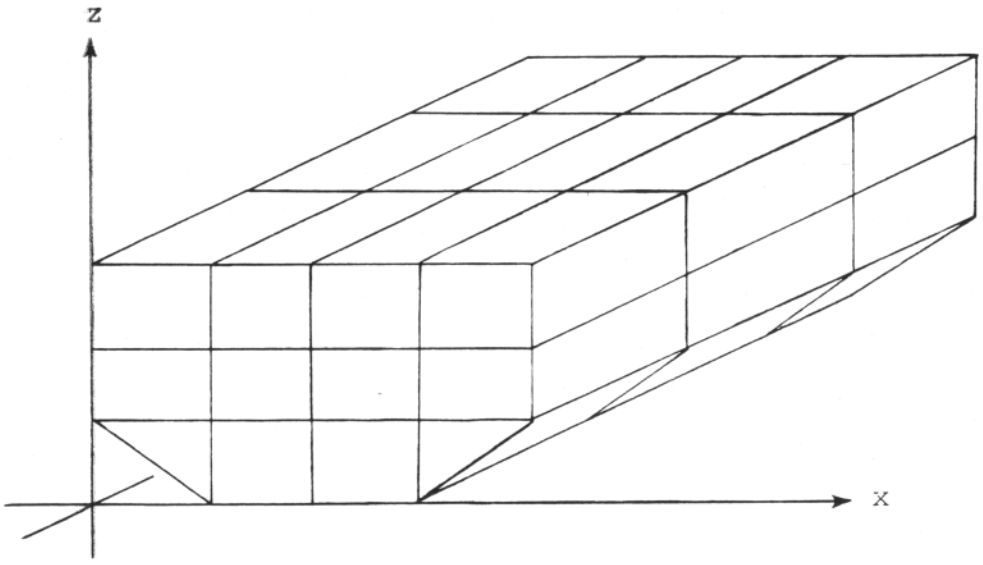

Figure 4. Typical Division of the Cargo Compartment Walls into Panels.

panels as shown in Figure 4. The number of panels for each plane can be varied to obtain the desired spatial resolution of temperature. The code divides each plane into panels automatically, computing panel dimensions, areas, center points, and surface normal vectors at the start of the simulation. Panel dimensions are selected to produce panels of approximately equal length and width. The method for computing the panels' temperatures and their exchanges of heat with the compartment interior is given in Section 2.9.

2.3 GOVERNING EQUATIONS OF THE COMPARTMENT ATMOSPHERE

Application of the laws of conservation of mass, species, and energy to each control volume forming the hot and cool zones results in the governing differential equations of the model. Since both zones are assumed to have no net overall velocity, conservation of momentum for each zone yields no useful information. The conservation equations are (see the Nomenclature for the definition of the symbols)

(1) $\frac{d}{dt} M_h = G_{vh} + G_{fh} + G_{hf}$ (mass, hot zone)

(2) $\frac{d}{dt} M_c = G_{vc} + G_{fc}$ (mass, cool zone)

(3) $\frac{d}{dt} M_{jh} = G_{jvh} + G_{jfh} + G_{jhf}$ (species j, hot zone)

(4) $\frac{d}{dt} M_{jc} = G_{jvc} + G_{jfc}$ (species j, cool zone)

(5) $\frac{d}{dt} I_h + V_h \frac{dP}{dt}$ (energy, hot zone)

$$= \dot{I}_{vh} + \dot{I}_{fh} + \dot{I}_{hf} + \dot{Q}_{wh} + \dot{Q}_{rih} - \dot{Q}_{roh}$$

(6) $\frac{d}{dt} I_c + V_c \frac{dP}{dt} = \dot{I}_{vc} + \dot{I}_{fc} + \dot{Q}_{wc}$ (energy, cool zone)

Each of the flow terms, the G's, $\dot{I}$'s, and $\dot{Q}$'s, on the right of Equations (1-6) have forms that are ultimately expressed in terms of the dependent variables of the problem: the zone gas densities, ρ_h and ρ_c; volumes, V_c and V_h; species mass fractions, Y_{jh} and Y_{jc}; and the temperature in each zone, T_h and T_c.

In principle, we could write expressions of the form of Equations (3) and (4) for each chemical species produced by the fire and each species present in the original compartment air. In practice, it is sufficient to account for only the six major constituents: nitrogen, oxygen, carbon dioxide, water, fuel, and "smoke." Therefore, we have six equations of type (3) and six of type (4) in the governing set. Further discussion of the chemistry used in the model is given in Section 2.7.

The volumes of the zones are related by the fact that the total volume of the compartment must remain constant:

$$V_t = V_c + V_h \quad . \tag{7}$$

In this expression we regard the volume of gas in the flame and plume as negligible. We also assume that the gas in each zone behaves as an ideal gas with constant specific heat, and so $I_h = c_{ph}T_h$ and $I_c = c_{pc}T_c$.

Another characteristic assumption of zone modeling is that, for the purposes of defining the thermodynamic properties of each zone, any spatial variation in the interior pressure is negligible with respect to the total value of the pressure. Therefore, we take the pressure in both zones as equal and employ the gas law to relate pressure, density, temperature, and species mass fraction:

$$P = \rho_h R_h T_h \quad , \tag{8}$$

where

$$R_h = \bar{R}/\left(\sum_{j=1}^{6} Y_{jh}\, \omega_j\right) \quad ; \tag{9}$$

and

$$P = \rho_c R_c T_c \quad , \tag{10}$$

where

$$R_c = \bar{R}/\left(\sum_{j=1}^{6} Y_{jc}\ \omega_j \right) \quad . \tag{11}$$

The symbol $\bar{R}$ is the universal gas constant, 8315 Joule/kg-mole/K, and ω_j represents the molecular weight of each gas species. The definitions of density and mass fraction relate these quantities to the mass and volume of each zone:

$$\rho_h = M_h/V_h \quad , \qquad Y_{jh} = M_{jh}/M_h \quad , \tag{12}$$

and

$$\rho_c = M_c/V_c \quad , \qquad Y_{jc} = M_{jc}/M_c \quad . \tag{13}$$

For the purposes of the numerical solution of the equations, it is better to use the pressure difference between the interior and exterior rather than the total pressure as one of the dependent variables. This is because a small pressure difference (in comparison to the total pressure) can cause a very large flow through a vent. Consequently, if the total pressure is used, it must be known to much greater precision than all the other variables. If, on the other hand, we write P in Equations (8) and (10) as

$$P = P_{ext} + \Delta P \quad , \tag{14}$$

where P_{ext} is pressure exterior to the compartment (a constant) and ΔP is the interior-exterior pressure difference, then ΔP need only be known to a precision equal to the other variables. We use ΔP throughout the model as the pressure variable. When the total pressure is required it is found from Equation (14).

One additional important quantity is the position of the hot zone-cool zone interface. This is specified by giving the

thickness of the cool zone, Z_c. If the compartment has a rectangular vertical cross-section, Z_c is found quickly from the cool zone volume by

$$Z_c = V_c/A \tag{15}$$

where A is the compartment horizontal cross-sectional area. When the compartment shape is not rectangular, for example, the typical shape shown in Figure 3, Z_c may still be obtained from V_c but an implicit relation involving the vertical cross-section shape must be used. Details of the method of computing Z_c in this case are found in the Appendix.

2.4 VENTILATION

Cargo compartments receive ventilation by forced air systems or by infiltration leakage. The CCFM can handle either type of ventilation separately or both types combined. The position and size of vent openings or leakage areas are specified in the input. Forced air (fixed flow) systems are treated by specifying the volume flow rate, either positive or negative, through the vent. Infiltration and flow out exhaust vents that is not forced (free flow) are computed using a simple orifice flow expression involving the interior - exterior pressure difference. The zone into which ventilation air flows or from which gas is drawn is determined by the location of the vent center point. When the center point is in a zone the entire vent area is assumed to be within that zone, so that at a given time a vent may exchange gas with either the hot zone or cool zone but not with both at once. When more than one vent opening lies within a zone, the vent flow terms, G_{vh}, G_{vc}, $\dot{I}_{vh}$, etc., are merely the algebraic sums of the terms for each vent.

Forced flow through vents is specified by the volume flow rate given in the input. The flow rate can be positive to indicate exterior air being forced into the compartment, or negative

to indicate compartment air being withdrawn. When the flow rate is positive, the inflowing gas density, temperature, and composition are those of the exterior air. When the flow is out, the density, temperature, and composition are those from the particular zone in which the opening lies. If the flow is out of the compartment, the mass flow rate out will vary depending upon the change in the zone density. The mass flow rate for the forced ventilation case is given by

$$G_v = \rho \dot{V} \quad . \tag{16}$$

The energy flow through the vent is found by multiplying the mass flow rate by the appropriate specific enthalpy of the flowing gas, that is

$$\dot{I}_v = c_p T \, G_v \tag{17}$$

where c_p, the gas heat capacity, is taken to be constant, and has the value for air at room temperature, 1004 J/(kg-K). T is the temperature of the incoming or outgoing flow.

When the flow through a vent is driven by the pressure difference between the interior and exterior, the Bernoulli equation gives the mass flow rate

$$G_v = C A_v (2\rho \Delta P)^{1/2} \quad . \tag{18}$$

The constant C in Equation (18) is an orifice coefficient whose value is taken to be 0.68. The energy flow rate is found again from Equation (17).

2.5 GAS ZONE RADIATION

As the smoke-filled hot zone rises in temperature, it will radiate a significant amount of energy to its surroundings. This radiation loss, $\dot{Q}_{roh}$ on the right hand side of Equation (5), figures strongly in determining the hot zone temperature. The hot zone will also absorb energy radiated from the fire flames or from other sources, and so the absorption term, $\dot{Q}_{rih}$ in

Equation (5), must also appear in the zone energy balance. Similar terms for the absorbed and emitted radiation for the cool zone could appear in Equation (6). However, for this version of the CCFM, the cool zone is assumed to be totally transparent to radiation and the terms are neglected. (These terms, set to zero, have been included in the computer code in anticipation of refinements which will take into account cool zone radiation.)

To compute the radiation emitted by the hot zone we assume that the zone emits and absorbs radiation as a gray gas with an absorption coefficient proportional to the zone's smoke concentration. The emittance is found using the mean beam length approximation [Ref. 5] for a gas volume of rectangular shape. This emittance is given by

$$\varepsilon = 1 - \exp(-\bar{k}_h L) \tag{19}$$

The mean beam length, L, is found from the expression

$$L = 3.6\ V/A_s \tag{20}$$

where V is the zone volume and A_s is the zone surface area. The emitted radiation is then computed from

$$\dot{Q}_{roh} = \varepsilon \sigma A_s T_h^4 \tag{21}$$

where T_h is the hot zone temperature and σ is the Stefan-Boltzmann constant, 5.67×10^{-8} W/(m^2-K^4).

The hot zone absorption coefficient, $\bar{k}_h$, can be related to the mass fraction of smoke in the hot zone by assuming that for radiation effects the smoke consists primarily of soot. Milter and Emmons [Ref. 6] give a rough estimate of soot density as 2,000 kg/m^3. From this we may estimate the volume fraction of soot as

(22) $$f_v = (\rho_h/\rho_{soot})Y_s \quad .$$

Hottel and Sarofim [Ref. 7] give a typical relationship between the spectral absorption coefficient and wavelength as

(23) $$k_\lambda \simeq 7f_v/\lambda$$

where k_λ is in meters^{-1} and λ is in meters. Most of the radiation will be in the infrared region from 0.8 to 10 micrometers so that an average absorption coefficient integrated over this region is

(24) $$\bar{k}_h = \int_{0.8\times10^{-6}}^{10\times10^{-6}} k_\lambda \, d\lambda \Big/ \int_{0.8\times10^{-6}}^{10\times10^{-6}} d\lambda \quad ,$$

or, carrying out the integration using Equation (23),

(25) $$\bar{k}_h = 1.92 \times 10^6 f_v \quad .$$

Next, using the definition of the mass fraction, we can express the average hot zone absorption coefficient in terms of the hot zone density and the smoke mass fraction as

(26) $$\bar{k}_h = 961\rho_h Y_s \quad .$$

The gaseous combustion products, particularly CO_2 and H_2O, accumulating in the hot zone will also emit significant radiation. If the smoke concentration is low this gas band radiation can be the major fraction of the hot zone radiant output. Detailed band radiation calculations are not warranted for a model of our level of approximation, so we have chosen to follow earlier practice [1] by adding a term to (26) to account for the gas contribution. A rough approximation of the effective value of $\bar{k}$ for a typical mix of compustion gases is 0.33 m^{-1}. Therefore the final expression for the hot zone absorption coefficient is

(27) $$\bar{k}_h = 961\rho_h Y_s + 0.33 \quad .$$

The hot zone absorbs radiation from the compartment interior surfaces and from the fire flames. In this version we neglect the flame radiation, primarily for convenience of computation, and account only for the radiation from the interior surfaces. To compute the rate of radiation absorbed by the hot zone, the mean beam length and spectrally gray absorption coefficient approximations used in the emmission term are applied once again. That is, the absorption term is written as

$$\dot{Q}_{rih} = \varepsilon \sigma A_s T_{ic}^4 \tag{28}$$

where T_{ic} is a characteristic interior surface temperature. This temperature is found from the area weighted average of the individual panel temperatures:

$$T_{ic}^4 = \left(\sum_{j=1}^{n_p} A_{pj} T_{pj}^4\right) / \left(\sum_{j=1}^{n_p} A_{pj}\right) \quad . \tag{29}$$

Note that the above analysis assumes that the view factor between each interior radiating surface and the hot zone is unity. This results in an overestimate for the radiation arriving from panels in contact with the lower zone, but the task of computing each view factor is too complex to be practical and so we make the unity view factor approximation. Further discussion of the radiation balance of the interior surfaces is given in Section 2.9.

Before closing this section we should mention that a more sophisticated and potentially much more accurate method of computing the hot zone radiation has been presented by Modak [Ref. 8]. Although Modak's method was developed specifically for zone models, we judged that it requires too much computer time and storage space for our application.

2.6 FIRE FLAMES AND PLUME

Because the emphasis in the CCFM is on the effects of reduced oxygen concentration (vitiation) on the fire development,

the choice of a model for the flame and plume structure is critical. Treatments of the flame and plume in most existing zone models have lacked combustion models sufficient to account for the effects of vitiation. The simple point-source plume equations used in Reference 4, for example, have no explicit combustion model at all. Steward [Ref. 9] constructed a flame-plume model with an explicit combustion process which has been used in several zone models. The model is successful in predicting trends in the variation of flame heights with burning rate, but its assumption that all entrained oxygen is burned instantaneously at the point of entrainment results in unrealistically short flame heights and high flame temperatures. A further problem is that due to the instantaneous combustion assumption there is no oxygen remaining at the flame tip so the amount carried into the hot zone is underestimated.

A recent improvement in modeling the flame and plume of a turbulent pool fire was made by deRis [Ref. 10]. The model incorporates a stochastic approach to the turbulent mixing in the flame and plume column which allows fuel and oxygen to co-exist at a given height within the column. The rate of consumption of oxygen and fuel is controlled by the mixing model and, as one consequence, there can be a non-zero mass fraction of oxygen present at the flame tip. This results in a better estimate of the flame volume, the flame temperature, the composition of the gas carried into the hot zone, and, ultimately, of the hot zone itself.

In the subsections that follow we give a description of the deRis flame/plume model as applied to the two-zone situation of the CCFM. Section 2.6.1 gives the rudiments of the method and the expressions for the flame and plume properties for those regions of the fire lying below the zone interface. The modifications necessary to describe the fire column in the hot zone

and, in particular, the gas properties at the ceiling where the column empties into the hot zone, are given in Section 2.6.2. Beyond the modifications to accomodate the two-zone environment, we have altered deRis' original formulation by using an entrainment coefficient which is a function of axial location in the flames. This gives somewhat better agreement with experimental observations on pool fires as explained below.

2.6.1 The Fire in the Cool Zone

The deRis model uses the following information as input: the fire base radius, b_o; the mass gasification rate at the fire base, $\dot{M}_o$; the fuel vapor density, temperature, and velocity at the fire base, ρ_o, T_o, u_o, respectively. In addition we need the heat of combustion of the fuel, ΔH_c, and the fraction of ΔH_c that results in temperature rise of the gases, J. The factor J includes the effective combustion efficiency and the fraction of the heat release lost to flame radiation. We also employ two terms involving the stoichiometric fuel to oxygen ratios. The first, r_c, involves the fuel mass fraction at the fire base and the oxygen mass fraction in the lower zone, while the second, r_h, involves the oxygen mass fraction in the upper zone and the fuel mass fraction at the point where the fire column penetrates into the hot zone:

$$r_c = \frac{Y_{O_2 c}\, \nu_f \omega_f}{Y_{fo}\, \nu_{O_2}\, \omega_{O_2}} \tag{30}$$

$$r_h = \frac{Y_{O_2 h}\, \nu_f \omega_f}{Y_{fi}\, \nu_{O_2}\, \omega_{O_2}} \tag{31}$$

The use of r_h will be discussed in the next section.

The major dependent variable in the deRis model is ζ, the ratio of the mass flow in the fire column at height d above the base to the mass flow at the fire base:

(32) $$\zeta = \dot{M}(d) \; / \; \dot{M}_o$$

The formulation of the model results in an integral equation for determining ζ:

(33) $$\frac{d}{b_o} = \left(\frac{\pi \rho_o}{\rho_c} \right)^{1/2} \int_1^{\zeta} \left[\frac{1}{K(\alpha)} \right] \left[1 + A_o \int_1^{\alpha} f(\beta) d\beta \right]^{-1/5} d\alpha$$

where $$A_o = \frac{5}{2} \left(\frac{g b_o}{c_p T_c u_o^2} \right) \left(\frac{\pi \rho_o}{\rho_c} \right)^{1/2}$$

and $$f(\beta) = K(\beta)\beta \left\{ J Y_{fo} \Delta H_c \left[1 - (1+r_c) I(\beta) \right] + c_{po}(T_o - T_c) \right\}$$

and $$I(\beta) = \int_{\frac{r_c \beta}{(1+r_c)}}^{2.7} \left[\Psi - \frac{r_c \beta}{(1+r_c)} \right] \exp \left(- \sum_{n=0}^{6} a_n \Psi^n \right) d\Psi \quad .$$

Equation (33) as written applies strictly to that part of the fire column between the base and the zone interface, as is indicated by the appearance of the cool zone quantities ρ_c, T_c, and r_c. With modification Equation (33) can also be used in the hot zone, as will be explained in Section 2.6.2.

The above form for $I(\beta)$ is that presented by de Ris in [10]. We note that, since the coefficients a_n are constant, the integral for I may be regarded as a function of the term $r_c\beta/(1+r_c)$. By numerically integrating $I(\beta)$ over the range 0. to 2.7 and then curve fitting the results, an analytic approximation to $I(\beta)$ is obtained which is more efficient for use in the code:

(34) $$I(\beta) = \begin{cases} \exp(-c_e \gamma^2) & \gamma \geq 1.68 \\ \sum_{i=0}^{4} c_i \gamma^i & \gamma < 1.68 \end{cases}$$

where $\gamma = r_c\beta/(1+r_c)$.

The coefficients c_e and c_i are listed in the Appendix.

To solve for ζ we numerically evaluate the right hand side of Equation (33) using small steps of α until equality of the left and right sides is reached. Note that two nested numerical integrations are involved. Both integrations are performed by the trapezoid rule.

The quantity $K(\alpha)$ appearing twice in Equation (33) is the entrainment coefficient. In de Ris' original development K was taken to be constant throughout the length of the column. To improve the flame height and temperature predictions of the model we allow K to vary as a function of the fuel mass fraction in the flame following work by Tamanini [Ref 11]. The effect of varying K is to reduce the entrainment near the base of the fire. This lengthens the flame and lowers the flame temperature, bringing the model into closer agreement with the available experimental data. The functional form for K is given in the Appendix.

Once ζ is determined, the mass flow rate in the plume at any height $d + Z_b < Z_c$ is known. Since we also know the mass flow rate at the base of the fire, the difference between the mass flow rate at a height d and that at the base will be the mass entrainment rate between the base and d. This allows us to write equations for the entrained mass flow from either zone. For the part of the fire (flames and/or plume) which lies in the cool zone, the total entrained mass flow at height d is

$$G_{fc} = \dot{M}_o \, (\zeta - 1) \tag{35}$$

where $\zeta = \zeta(d)$. The fire column radius, b, at this height can be found from

$$\left(\frac{b}{b_o}\right)^2 = \frac{\zeta^2}{W} \frac{\rho_o}{\rho_c} \left[\frac{JY_{fo}\Delta H_c[1-(1+r_c)I(\zeta)] + c_{po}(T_o - T_c)}{\zeta c_{pc} T_c} + 1 \right] \tag{36}$$

where $W = \left[1 + A_o \int_1^{\zeta} f(\beta)d\beta\right]^{2/5}$.

Using the mass flow and the plume column radius allows us to solve for the density, velocity, and fuel mass fraction at d:

$$\rho = \left(\frac{b_o}{b}\right)^2 \rho_o \frac{\zeta^2}{W} ,$$

(37) $$u = \frac{\zeta \dot{M}_o}{(\pi b^2 \rho)} ,$$

$$Y_f = Y_{fo}(1+r_c)I(\zeta)/\zeta \quad .$$

And finally, the temperature in the plume may be obtained from the total energy flow rate given by

(38) $$\dot{Q}(\zeta) = \Delta H_c J Y_{fo} \dot{M}_o [1 - (1+r_c)I(\zeta)] + \dot{M}_o c_{po} (T_o - T_c) \quad .$$

The temperature in the flames or plumes at the height, d, can then be obtained from

(39) $$T = \dot{Q}(\zeta)/(\zeta \dot{M}_o c_p) + T_c \quad .$$

In the above expression, the variation of the specific heat of the plume gas, c_p, with temperature must be taken into account. The expression is then implicit in the plume temperature and must be solved by an iterative procedure. The procedure used in the CCFM is described in the Appendix.

To determine the total amount of mass, species, and energy removed from the cool zone by entrainment into the fire we evaluate Equations (33) and (35) with d equal to the distance between the fire base and the zone interface, that is, $d = Z_c - Z_b$. The mass flow ratio in the fire column at the zone interface found from Equation (33) is denoted ζ_i. The species and energy flow terms in Equations (4) and (6) are then written as

(40) $$G_{jfc} = Y_{cj} G_{fc}(\zeta_i) \quad ,$$

and

(41) $$\dot{I}_{fc} = c_{pc} T_c G_{fc}(\zeta_i) \quad .$$

2.6.2 The Fire in the Hot Zone

When the flames penetrate into the hot zone there will be a change in the combustion due to the difference in composition between the hot and cool zones. To account for this the model treats the part of the fire in the hot zone as if it were a separate fire with its base in the plane of the zone interface. Equations (32) through (39) are solved for the flame and plume quantitites, but with the properties of the hot zone substituted for those of the cool and the column properties at the interface substituted for the base values. That is, r_h is substituted for r_c, T_h for T_c, ρ_h for ρ_c, Y_{fi} for Y_{fo}, ρ_i for ρ_o, etc. The mass flow ratio is computed based on the ratio of the mass flow at a position above the zone interface to that at the zone interface:

$$\eta = \dot{M}(d) \; / \; \dot{M}_i \tag{42}$$

where d is now measured from the interface. Note that η has meaning only in the hot zone. By the same argument used for Equation (35) we can write for the total gas entrained into the hot zone the expression

$$G_{fh} = \dot{M}_i \; (\eta - 1) \quad , \tag{43}$$

where η is now found from Equation (42). The plume properties in the hot zone are then obtained analogously to Equations (36) through (39). The mass species, and energy flows from the hot zone into fire column are written as

$$G_{jfh} = Y_{hj} \; G_{fh} \; (\eta_c) \tag{44}$$

and

$$\dot{I}_{fh} = c_{ph} \; T_h \; G_{fh} \; (\eta_c) \; . \tag{45}$$

G_{fh} is evaluated using the distance between the interface and the compartment ceiling where the mass flow ratio is η_c.

When the plume strikes the ceiling, the total mass and energy flows in the plume at that level are assumed to enter and

mix with the hot zone. The terms in the governing equations which represent these hot zone inflows are G_{hf} and $\dot{I}_{hf}$. Values for these terms are readily obtained once η_c is known by using Equation (42) and the analogue of Equation (38) for the plume in the hot zone.

2.6.3 Species Concentrations

In addition to expressions for the flame/plume temperature, radius, and density, we need expressions for the oxygen, fuel, and product concentrations in the flames and plume in order to find the quantity of these materials entering the hot zone. To obtain expressions for the plume constituents, we must consider two general cases: (1) the flame tip lies below the zone interface, and (2) the tip is above the interface. The flame tip is defined as the point at which the mass fraction of fuel in the plume, Y_f, reaches zero.

The mass fraction of fuel in the plume at the zone interface is computed using Equation (37) evaluated at ζ_i (mass flow ratio at the interface):

$$Y_f(\zeta_i) = Y_{f_o} (1 + r_c) I(\zeta_i) / \zeta_i \quad . \tag{46}$$

The flame tip location then determines which expression to use for the plume's oxygen mass fraction at the zone interface:

$$Y_{O_2}(\zeta_i) = \begin{cases} Y_{O_2 c} [1 - (1.19/\gamma_i)] & , \; Y_f(\zeta_i) = 0 \\ Y_{O_2 c} \left(\frac{1}{\gamma_i}\right) \int_0^{\gamma_i} [\gamma_i - \psi] \exp\left[-\sum_{n=0}^{6} a_n \psi^n\right] d\psi & , \; Y_f(\zeta_i) > 0 \end{cases} \tag{47}$$

where $\gamma_i = r_c \zeta_i / (1+r_c)$. The species mass fractions of the plume's remaining constituents at the zone interface are computed as follows:

$$Y_{N_2}(\zeta_i) = [Y_{N_2}(1) + (\zeta_i - 1) Y_{N_2 c}] / \zeta_i \quad , \tag{48}$$

$$(49)\quad Y_{CO_2}(\zeta_i) = \frac{[1 - Y_f(\zeta_i) - Y_{O_2}(\zeta_i) - Y_{N_2}(\zeta_i)]}{1 + \frac{9}{22}\frac{\nu_{H_2O}}{\nu_{CO_2}} + \frac{\omega_f}{44}\frac{\nu_S}{\nu_{CO_2}}} \quad ,$$

$$(50)\quad Y_{H_2O}(\zeta_i) = \frac{9}{22}\frac{\nu_{H_2O}}{\nu_{CO_2}} Y_{CO_2}(\zeta_i) \quad , \text{ and}$$

$$(51)\quad Y_S(\zeta_i) = \frac{\omega_f}{44}\frac{\nu_S}{\nu_{CO_2}} Y_{CO_2}(\zeta_i) \quad .$$

In the above, $Y_{N_2}(1)$ is the nitrogen fraction in the fuel vapor gases at the fuel surface, if any. The forms for the product concentrations, Y_{CO_2}, Y_{H_2O}, and Y_S, result from the assumptions of the combustion chemistry given in Section 2.7.

The hot zone equivalent of Equation (46), evaluated at η_c (mass flow ratio at the ceiling), is used to obtain the plume's fuel mass fraction at the compartment ceiling:

$$(52)\quad Y_f(\eta_c) = Y_f(\zeta_i)\,(1+r_h)\,I(\eta_c) / \eta_c \quad .$$

The flame tip location controls the computation of the plume's oxygen mass fraction at the ceiling:

$$(53)\quad Y_{O_2}(\eta_c) = \begin{cases} [Y_{O_2}(\zeta_i) + (\eta_c - 1)\,Y_{O_2h}]/\eta_c \quad , & Y_f(\zeta_i) = 0 \\ Y_{O_2h}\,[1 - (1.19/\gamma_c)] \quad , & Y_f(\zeta_i) > 0 \text{ and } Y_f(\eta_c) = 0 \\ Y_{O_2h}\left(\frac{1}{\gamma_c}\right)\int_0^{\gamma_c} [\gamma_c - \psi]\,\exp\left[-\sum_{n=0}^{6} a_n \psi^n\right] d\psi \quad , & Y_f(\eta_c) > 0 \end{cases}$$

where $\gamma_c = r_h \eta_c / (1+r_h)$. The plume's other species mass fractions at the ceiling can then be computed:

$$(54)\quad Y_{N_2}(\eta_c) = [\,Y_{N_2}(\zeta_i) + (\eta_c - 1)\,Y_{N_2h}\,] / \eta_c \quad ,$$

$$(55) \quad Y_{CO_2}(\eta_c) = \frac{[1 - Y_f(\eta_c) - Y_{O_2}(\eta_c) - Y_{N_2}(\eta_c)]}{\left(1 + \frac{9}{22}\frac{\nu_{H_2O}}{\nu_{CO_2}} + \frac{\omega_f}{44}\frac{\nu_S}{\nu_{CO_2}}\right)} \quad ,$$

$$(56) \quad Y_{H_2O}(\eta_c) = \frac{9}{22}\frac{\nu_{H_2O}}{\nu_{CO_2}} Y_{CO_2}(\eta_c) \quad , \text{ and}$$

$$(57) \quad Y_S(\eta_c) = \frac{\omega_f}{44}\frac{\nu_S}{\nu_{CO_2}} Y_{CO_2}(\eta_c) \quad .$$

The integral in Equations (47) and (53) may be approximated by curve fitting as was the $I(\beta)$ integral of Equation (33). Details of this approximation are given in the Appendix.

The flow of each species into the hot zone at the point where the fire column strikes is found by multiplying the mass flux in the plume at that point by the particular species mass fraction of interest evaluated at η_c. The product is the term G_{jhf} of the species governing equations for the hot zone.

2.7 COMBUSTION MODEL

The rate of consumption of oxygen and fuel, and of the production of combustion products, particularly smoke, is determined by our assumption of a combustion reaction equation. In keeping with the level of sophistication of the other parts of the CCFM, a single step global combustion reaction is an appropriate model for the fire chemistry. The reaction is assumed to occur instantaneously once the fuel and oxygen are mixed by the turbulent processes of the fire plume.

We adopt the following form for the combustion reaction:

$$(58) \quad \nu_f C_aH_bO_c + \nu_{O_2} O_2 \rightarrow \nu_{CO_2} CO_2 + \nu_{H_2O} H_2O + \nu_s C_aH_bO_c \; .$$

The combustion products on the right hand side are carbon dioxide, water, and "smoke" which is assumed, for lack of better information, to have the same overall molecular composition as the fuel. The fuel may contain carbon, hydrogen, and oxygen. Most fuels, such as cellulosics and common polymers, are hydrocarbons made primarily of these elements. When preparing input data for a specific fuel, the user selects the values of a, b, and c which best describe the composition of the fuel and then balances the reaction equation to obtain values for the stoichiometric coefficients ν_f, ν_{O_2}, etc. The stoichiometric coefficients and the molecular weight assumed for the fuel are the only input items required to describe the reaction chemistry.

It can be seen from Equation (58) that, with the exception of smoke, we assume complete combustion of the fuel to CO_2 and H_2O. Other products, particularly carbon monoxide, which usually are present in significant amounts in this type of fire have not been included. We have done so for two reasons: (1) there is little data on CO yields for most materials (and the yield will be expected to change as vitiation increases), and (2) our interest in the CCFM is in burning rate predictions, not in the levels of particular toxic products.

With our assumption of the combustion model presented we can explain the relationships of Section 2.6.3 which give the product concentrations in the flames and plume in terms of the oxygen and nitrogen concentrations. Nitrogen is an inert entrained into the fire column at a rate proportional to the zone concentration. Because the sum of all mass fractions in the plume is one, the mass fraction of the products taken as a unit is

$$Y_p = 1 - Y_f - Y_{O_2} - Y_{N_2} \quad , \tag{59}$$

where $Y_p = Y_{CO_2} + Y_{H_2O} + Y_S$. From the stoichiometry of the reaction the mass fractions of carbon dioxide and water in the plume are related by

$$(60) \qquad Y_{H_2O} = \frac{18}{44} \frac{\nu_{H_2O}}{\nu_{CO_2}} Y_{CO_2} \quad ,$$

and those of smoke and CO_2 are related by

$$(61) \qquad Y_S = \frac{\omega_f}{44} \frac{\nu_S}{\nu_{CO_2}} Y_{CO_2} \quad .$$

Substituting into the definition of Y_p and then applying Equation (59), we can write an expression for the CO_2 mass fraction as

$$(62) \qquad Y_{CO_2} = \frac{1 - Y_f - Y_{O_2} - Y_{N_2}}{\left(1 + \frac{9}{22} \frac{\nu_{H_2O}}{\nu_{CO_2}} + \frac{\omega_f}{44} \frac{\nu_S}{\nu_{CO_2}} \right)} \quad .$$

Therefore, once the reactant and the inert concentrations are known, Equations (60) through (62) give the product concentrations. We should note that these relationships hold because we assume that the fire is the only source of the product species, and so they are always present in the same ratio whether in the flames, plume, or hot zone. If there were other, independent sources of smoke, CO_2, or water, we could not use this simplifying argument.

2.8 RADIATIVE AND CONVECTIVE HEAT TRANSFER TO THE FIRE FUEL

The central item of interest in the CCFM is the prediction of the burning rate of the fire. The burning rate, either measured as the mass vaporization rate of the fuel or as the total heat release rate, is determined by the amount of energy fed back to the fuel from the surroundings. The majority of this energy, of course, comes from the flame directly adjacent to the

fuel surface. For fires on the scale of interest to this problem - base radii on the order of one meter - both radiation and convection to the fuel surface are significant. The treatment of the fuel surface heat flux used in the CCFM follows the work of deRis [Ref.12] who developed practical engineering methods for predicting burning rates of polymer pool fires.

2.8.1 Flame Radiation to the Fuel

For flame radiation to the fuel, we use a uniform gray gas, mean beam length approach and model the flame volume as a right circular cone of height, h_f, and base radius, b_0. The flame base is always assumed to be a circular area with the fuel surface facing horizontally upward. The volume of the flame cone is then

$$V_f = \frac{1}{3}\pi b_o^2 h_f \quad , \tag{63}$$

and the total surface area is

$$A_f = \pi b_o^2 + \pi b_o (b_o^2 + h_f^2)^{1/2} \quad . \tag{64}$$

As in the case of the hot zone radiation, the mean beam length of the flame is found from

$$L_f = 3.6 V_f / A_f \quad . \tag{65}$$

The expression for the radiant flux from the flame to the fire base is then

$$\dot{q}''_{rfb} = \sigma \bar{T}_f^4 [1 - \exp(-\bar{k}_f L_f)] \quad . \tag{66}$$

In the expression above, the absorption coefficient and the flame temperature are average values for the entire flame volume. For the temperature, $\bar{T}_f$, the flame/plume structure equations of section 2.6 are used to compute the temperature at five equally spaced locations along the flame axis. These five values are

then averaged. Tests of this procedure versus flame temperature data quoted by de Ris [Ref 12] and experiments by McCaffrey [Ref 13] showed that the average value computed was consistently about 200K lower than the measured values. Consequently, 200K is added to the five point average to improve the estimate.

Santo [Ref.14] has studied the influence of oxygen depletion on the radiative properties of fires of the polymer polymethylmethacrylate (PMMA). His measurements provide an estimate of the change in absorption coefficient for these flames as a function of the oxygen concentration. Santo observed a decrease in the emissivity of the flames as the available oxygen decreased due apparently to the decrease in the amount of soot produced.

From Santo's data we compute an average absorption coefficient for the flame volume using the oxygen mass fraction in the entrained air. Santo's experiments ranged over a relatively narrow band of oxygen mass fraction: from 0.209 to 0.180 by volume. We assume that there is a lower limit on the absorption coefficient imposed by the gas band radiation from CO_2 and water vapor. This limit is taken to be 0.33 m^{-1}. Santo's data, with the lower limit added, can be fit with a hyperbolic tangent function. This relationship between $\bar{k}_f$ and the oxygen mass fraction is

$$\bar{k}_f = 0.67 \tanh(63.615 Y_{O_2} - 13.094) + 1.0 \quad . \tag{67}$$

When the flame is split between zones, we compute one value of $\bar{k}_f$ for each part of the flame using the Y_{O_2} for the appropriate zone. We then find an average absorption coefficient using a weighted average involving the amount of the flame in each zone. This expression is

$$(\bar{k}_f)_{avg} = \left(\frac{d_h}{h_f}\right) \bar{k}_f(Y_{O_2 h}) + \left(\frac{d_c}{h_f}\right) \bar{k}_f(Y_{O_2 c}) \quad , \tag{68}$$

where d_h is the flame length in the hot zone and d_c is the flame

length in the cool zone.

2.8.2 Convective Heat Flux to the Fuel

The other major contribution of heat from the flames to the fuel surface is the convective flux. In his work deRis proposed a stagnant film model for this process which represents the convective flux as

$$(69)\quad \dot{q}''_c = \left[\Delta H_c(1-\chi_r/E_c)r - c_{po}(T_0-T)\right] \frac{\dot{m}''_g}{\exp(\dot{m}''_g c_{po}/h)-1} \quad ,$$

where T and r correspond to the zone in contact with the fire base (T_c and r_c for the cool zone; T_h and r_h for the hot zone). The major point of interest in the above equation is that the convective heat flux, $\dot{q}''_c$, is a function of the mass gasification rate, $\dot{m}''_g$. We require, therefore, an estimate of the mass gasification rate before we can calculate $\dot{q}''_c$. To do this we use a first guess of $\dot{m}''_g$ (from the previous time step or from the input) and iterate to evaluate the convective flux and the mass gasification rate simultaneously. The details of computing $\dot{m}''_g$ are given in Section 2.8.4. In Equation (69) we must have an estimate for the ratio h/c_{po}. Estimates by deRis show this ratio to be about 10 ($g/s\text{-}m^2$) for typical fuels and we use this estimate in the CCFM for all cases.

2.8.3 Radiation from the Hot Zone to the Fire Base

In addition to the radiation and convection from the flames to the fuel, there is a significant amount of radiation from the hot zone to the fire base which acts as a major accelerating factor for the fire. The methods for calculating this radiation have been presented by a number of workers, for example, Reference 3. Following this work we make the usual gray gas, mean beam length radiation approximation and then calculate a view factor from the fire base to the hot zone. The view fac-

tor is computed by dividing the upper zone into four segments. The segments meet along a line directed upward from the center of the fire base. Each segment is then treated as a rectangular volume with one corner above the fire base center. The somewhat cumbersome, but straightforward expression for the view factor from the fire to each segment, i, is

$$F_i = \frac{1}{2\pi}\left[\frac{x_i}{D_{x_i}}\tan^{-1}\left(\frac{y_i}{D_{x_i}}\right) + \frac{y_i}{D_{y_i}}\tan^{-1}\left(\frac{x_i}{D_{y_i}}\right)\right] \tag{70}$$

where x_i and y_i are the dimensions of the segment in the plane parallel to the fire base, $D_{x_i} = (D^2+x_i^2)^{1/2}$, $D_{y_i} = (D^2+y_i^2)^{1/2}$, and D is the distance from the fire base to the zone interface. The mean beam length of each segment must also be computed:

$$L_i = \frac{2\, x_i\, y_i\, z_h}{z_h(x_i + y_i) + x_i y_i} \quad , \tag{71}$$

where x_i and y_i are as above, and z_h is the hot zone thickness. The radiation flux from the hot zone to the base is then

$$\dot{q}''_{rhb} = \sum_{i=1}^{4} F_i \left[1 - \exp(-\bar{k}_h L_i)\right] \sigma T_h^4 \quad . \tag{72}$$

2.8.4 Fuel Vaporization

With the above method for calculating the heat input to the fuel, we now have the information required to find the fuel vaporization rate. In the CCFM we have taken the approach of modeling the fuel vaporization as a simple phase change of a pure substance. This model is probably more appropriate to polymer fuels than it is to cellulosic fuels where charring and other more complex phenomena might take place as the fuel gasifies. There are, however, no more sophisticated models (to our knowledge) which could be applied to the problem within the scope of the model. Thus, using a simple phase change approach, we need only specify an effective latent heat of

vaporization, L_v, to write the mass gasification rate of the fuel per unit area as

$$(73) \qquad \dot{m}''_g = \frac{1}{L_v} (\dot{q}''_{rfb} + \dot{q}''_{rhb} + \dot{q}''_c - \dot{q}''_{rr}) \quad .$$

On the right hand side of the above expression are three terms representing the heat flux from the flames and from the hot zone to the fuel surface. The fourth term represents a not-insignificant surface reradiation. The value of $\dot{q}''_{rr}$ will depend upon the emittance and temperature of the fuel surface. Since little information on these quantitites is available, we assume that the surface is black, and we specify an average, constant surface temperature in the input so that $\dot{q}''_{rr}$ is σT_0^4.

It was stated in Section 2.8.2 that the convective feedback term $\dot{q}''_c$ involves the mass gasification rate $\dot{m}''_g$, and, therefore, in order to solve for both of these quantities an iterative technique is necessary. This technique is implemented as follows. We first compute the three radiation terms. We then use an initial estimate of 10^{-2} kg/m^{2}s for the mass gasification rate and solve for a first estimate of $\dot{q}''_c$. We then insert that estimate into Equation (73) to update the mass gasification rate. The updated rate is used next for a new estmate of $\dot{q}''_c$, and the iterative loop is continued until the relative difference between the successive new and old estimates of the gasification rate is less than 5%. When this is accomplished we continue with the computations of the other fire quantities.

2.9 THERMAL RESPONSE OF THE COMPARTMENT LINING SURFACES

Cargo compartment walls and ceilings are normally fabricated of very thin fiber-reinforced polymer sheets. The flooring is usually made of sheet metal. Because of their light weight construction, the walls, ceilings, and floor will heat quickly during the development of the fire. As the temperature dif-

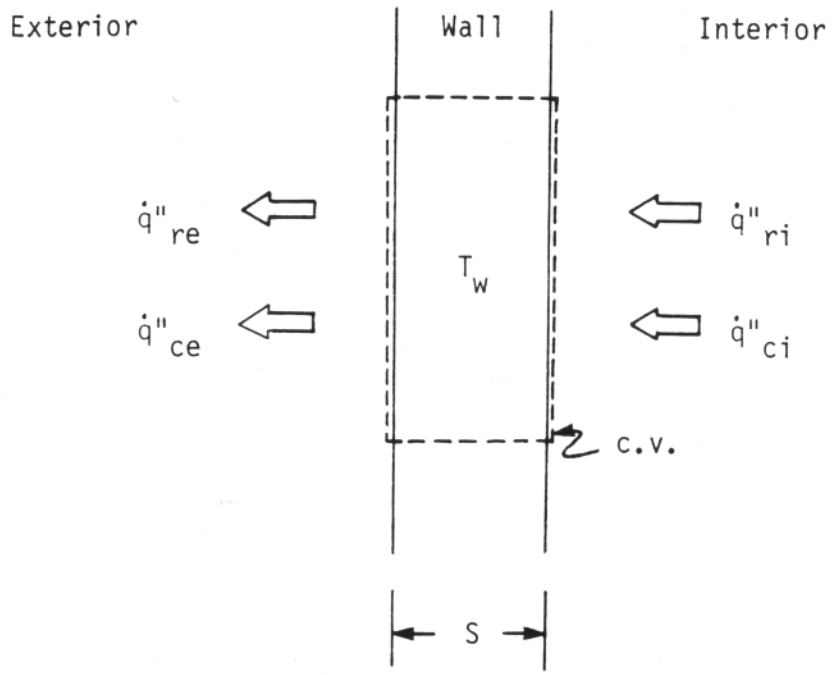

Figure 5. Energy Balance Applied to a Section of the Compartment Wall.

lateral conduction, that is, conduction within the material parallel to the faces, is negligible. We also neglect any effects from supports.

An energy balance applied to the control volume yields the following equation for the material temperature:

$$\frac{dT_w}{dt} = \frac{1}{c\rho s}\left(\dot{q}''_{ri} + \dot{q}''_{re} + \dot{q}''_{ci} + \dot{q}''_{ce}\right) \quad . \tag{74}$$

One equation of this type is written for each wall, ceiling, and floor panel in the CCFM. Each equation is solved for the new panel temperature at each time step. The four heat flux terms, $\dot{q}''_{re}$, $\dot{q}''_{ce}$, $\dot{q}''_{ri}$, and $\dot{q}''_{ci}$, are functions of the panel location, orientation, and the panel temperature, T_w. The following sections give the descriptions of how each of the four flux are obtained.

2.9.1 Exterior Surface Radiation

The exterior surface radiation, $\dot{q}''_{re}$, is obtained by assuming that the exterior surroundings of the compartment are at temperature, T_{amb}, and that the surface emits radiation with an emissivity of 0.8. The radiation term is therefore written

$$\dot{q}''_{re} = 0.8\sigma \left(T_{amb}^4 - T_w^4\right) \quad . \tag{75}$$

The view factor in the above expression is taken as unity, for we assume that the exterior surface of the panel sees only surroundings at temperature T_{amb}.

2.9.2 Exterior Surface Convection

To estimate the convective heat transfer from the compartment exterior we must first determine what flow conditions (laminar or turbulent, forced or natural convection) are likely to prevail on the various outside surfaces. The typical width of the separation between the compartment exterior and the fuselage

skin or the cabin floor is about 0.3 meters (1 foot). Air flow rates in this gap (deriving from the ventilation system) are between 5.7 and 8.5 cubic meters per minute (200 to 300 cubic feet per minute). For a representative compartment length of 5.5 meters (18 feet) this yields a characteristic velocity of only 0.3 meters per second (1.0 foot per second). Therefore, the Reynolds number for flow over a distance of this size would be no more than about 10^5, indicating that the flow should be mostly laminar.

At such low air velocities the heat transfer may be determined not by the forcing of the ventilation but by the natural convection from the hot compartment panels. Taking a typical temperature difference of 150K (270R) and a characteristic length of one meter (3.3 ft) gives a Grashof number of about 10^9, well into the transition region. Since transitional and turbulent free convection should dominate over laminar forced convection, we use free convection correlations for all exterior surfaces. All the correlations are to be found in the standard tests, for example Kays and Crawford [Ref. 16] or Krieth [Ref. 17].

Two expressions are used to compute the heat transfer coefficient, the choice between the two depending on the orientation of the surface. The angle of orientation is measured between the surface and the vertical as shown in Figure 6. For orientations between horizontal upward facing ($\theta = +90°$) and $\theta = +30°$, we approximate the change in h with a linear variation in θ by interpolating between expressions for $\theta = +90°$ and $\theta = +30°$ presented in [17]. Evaluated for air near room temperature, the expression is

$$h = (0.6 + 0.4\theta)(\Delta T)^{1/3} \tag{76}$$

where θ is in radians and ΔT is the difference between the surface and exterior air temperatures.

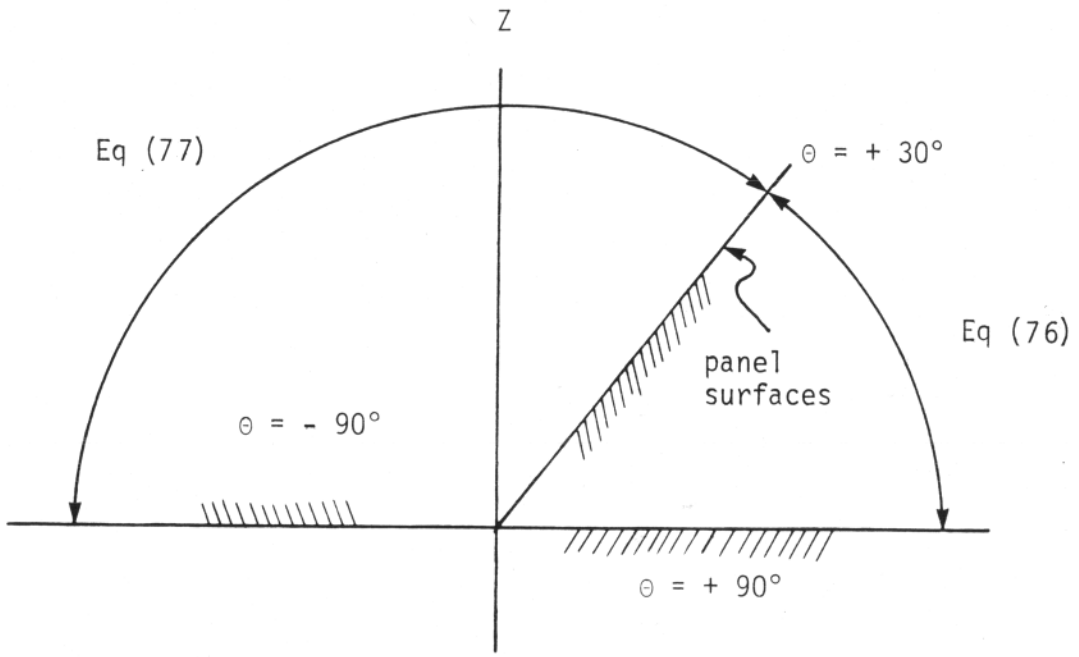

Figure 6. Range of Panel Surface Orientation.

All other orientations lie in the range of θ from +30° to -90°. For this range we adapt a correlation from [17] evaluated for air

$$h = 0.892(\cos\theta)^{2/3} (\Delta T)^{1/3} \quad . \tag{77}$$

Again θ is in radians and ΔT is the surface-exterior gas temperature difference. It is interesting to note that the length scale of the surface does not appear in either (76) or (77). This is due to the 1/3 power variation in the Grashof number in the correlations from which (76) and (77) were derived.

In Equation (77) $\cos\theta$, and thus h, will be zero at $\theta = -90°$. Further, the values for h may be very small for values near -90°. To provide a realistic lower limit when the surface orientation nears -90°, we adapt a correlation for laminar convection from downward facing horizontal plates given in [17],

$$h = 0.512(\Delta T)^{1/4} \quad . \tag{78}$$

The numerical coefficient in (78) arises by assuming a characteristic surface length of one meter and the properties of room temperature air.

2.9.3 Interior Surface Radiation

Because of the relatively small dimensions and high temperatures expected in a cargo compartment fire, the interior radiation exchange between the surfaces, the hot zone gas, and the flame make important parts of the thermodynamic model of the process. For the interior surfaces of wall panels, we account for radiation coming from the hot zone gas and radiation from the fire flame. We also include a term for radiation from other surrounding surfaces. This term, small during the latter stages of the fire where the flame and hot zone radiation dominate, is significant when the hot zone emission is small. To compute the incoming radiation from the hot zone gas we use a gray gas, mean beam length approximation similar in many respects to the computation of the hot zone to flame base flux.

In Figure 7, a panel in contact with the hot zone gas is shown. The total volume of the zone, assumed to be a rectangular solid, is divided into four sub-volumes which meet at the center point of the panel. Mean beam lengths for these sub-volumes are obtained by the following expressions:

(79) $$\ell_1 = 2LUA \;/\; [A(L+U)+LU] \quad ,$$

(80) $$\ell_2 = 2LDA \;/\; [A(L+D)+LD] \quad ,$$

(81) $$\ell_3 = 2DRA \;/\; [A(D+R)+RD] \quad , \text{ and}$$

(82) $$\ell_4 = 2URA \;/\; [A(U+R)+UR] \quad .$$

Since we have available the hot zone absorption coefficient, $\bar{k}_h$, calculated in Equation (27), we may then write the total emissivity for the incoming hot zone radiation as the sum of the contribution of each of the four sub-volumes:

(83) $$\varepsilon = 1-0.25\,(e^{-\bar{k}_h \ell_1} + e^{-\bar{k}_h \ell_2} + e^{-\bar{k}_h \ell_3} + e^{-\bar{k}_h \ell_4}) \quad .$$

The total incoming radiation then is obtained from assuming that the hot zone gas radiates as a gray body:

(84) $$\dot{q}''_I = \varepsilon\, \sigma\, T_h^4 \quad .$$

Radiation may also reach panels in contact with the hot zone from the flames. This is particularly significant when the hot zone is relatively transparent which may occur in the early stages of the fire. Accurately computing the radiation from the finite flame volume to the finite surface of the panel requires more effort than is practical for the CCFM. We have, therefore, adopted a simplified, approximate approach by assuming that the flames can be modeled as a point source of radiation and that the average radiant flux arriving at the surface of the panel is equal to that at the panel's center point. The total radiant power of the flames can be written as

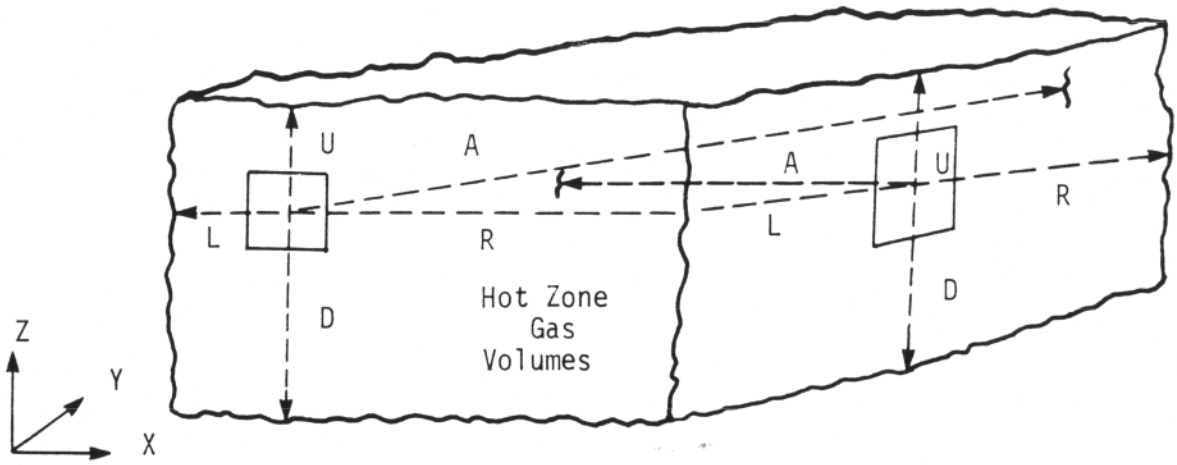

Figure 7. Hot Zone Dimensions for Computing the Zone Emittance.

(85) $$\dot{Q}_{Rf} = \chi_r E_c \Delta H_c \dot{M}_o$$

and the distance between the approximate center of the flames and the panel centerpoint is given by

(86) $$r_i = [(x_i-x_f)^2 + (y_i-y_f)^2 + (z_i-z_f)^2]^{1/2}$$

where x_i, y_i, and z_i are the panel center coordinates and x_f, y_f, and z_f are the fire center coordinates which we take to be the center of the fire base. We account for the relative orientation of the panel surface with respect to the line connecting the fire center to the panel center by computing the cosine of the angle Φ shown in Figure 8 as follows:

(87) $$\cos\Phi = [(x_f-x_i)n_x + (y_f-y_i)n_y + (z_f-z_i)n_z]/r_i$$

where (n_x, n_y, n_z) is the inward unit normal vector of the panel surface. The flame radiation to panel i is then, under this rough approximation,

(88) $$\dot{q}''_{II} = \left(e^{-\bar{k}_h r_i}\right)\frac{\dot{Q}_{Rf}}{r_i^2}\cos\Phi \quad .$$

Taking into account the flame radiation and the radiation from the hot zone gas, we compute the net radiation to the interior surfaces of panels in contact with the hot zone as

(89) $$\dot{q}''_{ri} = \dot{q}''_{I} + \dot{q}''_{II} + (1-\varepsilon)\sigma T_c^4 - 0.8\sigma T_w^4 \quad .$$

The third and fourth terms in (89) represent, respectively, an approximation for the total radiation arriving from cool zone surfaces and the radiation emitted by the panel.

For panels in contact with the cool zone we account for the incoming flame radiation and the radiation arriving from the hot zone. The difference in this case is that the view factor for a panel in the cool zone viewing the hot zone gas is not unity. The incoming flux to a cool zone panel is computed by the

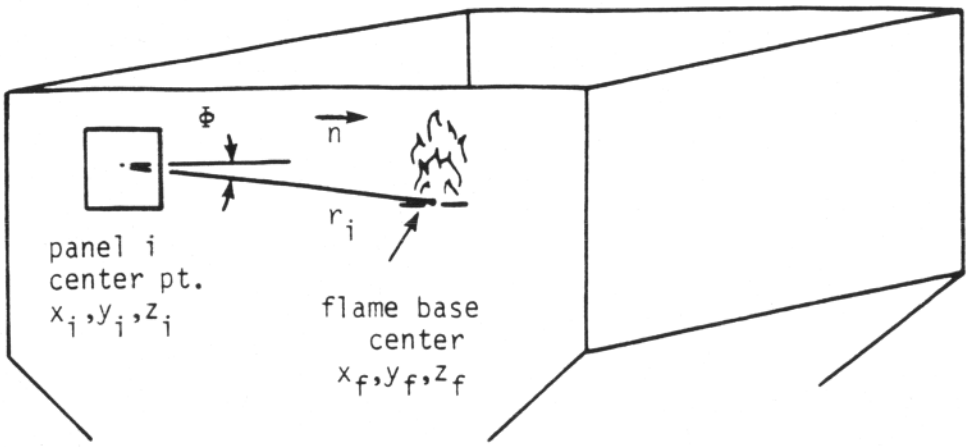

Figure 8. Quantities Used for the Flame-to-Surface Radiation.

method of Section 2.8.3 and then a correction is made if the panel does not face directly upward. The correction approximates the change in the view factor as the normal deviates from the vertical.

$$\dot{q}''_I = \frac{1}{3}\left(2 + \frac{n_z}{|\vec{n}|}\right)\dot{q}''_r \tag{90}$$

where $\dot{q}''_r$ is the flux for a panel whose surface normal is parallel to the z axis. If n_z is less than zero $\dot{q}''_I$ is taken as zero.

Radiation arriving at the surface of the panels and contact with the cool zone from the flames of the fire is handled by the point source approximation applied in the hot zone. The difference in this case is that we do not add the term for the attenuation through the hot zone gas. The net radiation to panels in the cool zone is then given by

$$\dot{q}''_{ri} = \dot{q}''_I + \dot{Q}_{Rf}\cos\Phi/r_i^2 + 0.8\sigma\left(T_c^4 - T_w^4\right) \quad . \tag{91}$$

The last term represents the difference between the incoming radiation from the other cool zone panels and the radiation emitted by the panel.

2.9.4 Interior Surface Convection

Convective heat transfer between the hot gases on the inside of the compartment and the walls, ceiling, and floor make a significant contribution to the energy equation for the hot zone. There will be large differences in the rates of heat transfer between the hot zone gas and the ceiling surfaces as a function of position over the ceiling. At the stagnation point where the rising flames and plume strike the ceiling, we expect, of course, a very large rate of heat transfer. As the impacting plume washes over the ceiling forming a radial ceiling jet, the rate of this transfer should diminish until at points far away from the plume impact the flow may be practically still and the

heat transfer rate relatively small. Therefore, a detailed accounting of a local heat transfer needs to be done in order to estimate the amount of heat loss from the hot zone and the distribution of ceiling temperature.

Cooper's analysis [Ref. 15] of the impact of fire plumes on ceilings offers a number of simple relationships for the heat transfer coefficient as a function of distance away from the plume impact point. Cooper's expressions are given in terms of the ratio of the radial distance, r_i, from the impact point to the distance between the ceiling and the fire base, H. In our analysis we assume that the entire ceiling lies within this radial spreading jet. We ignore the effect of the side walls on the radial jet.

Cooper divides the region from the impact point outward into three areas. Very close to the stagnation point, that is for values of r_i/H between 0 and 0.2, we use the following expression for the heat transfer coefficient:

$$h = 7.64\ \rho_h\ c_p\ V_p\ Re^{-0.5}\ [1 - (r_i/H)(5-0.39Re^{0.2})] \quad . \tag{92}$$

For r_i/H between 0.2 and 1.03 Cooper recommends

$$h = 0.21\ \rho_h\ c_p\ V_p\ Re^{-0.3}\ (r_i/H)^{-0.65} \quad . \tag{93}$$

Finally for r_i/H greater than 1.03, the following expression applies

$$h = 0.214\ \rho_h\ c_p\ V_p\ Re^{-0.3}\ (r_i/H)^{-1.2} \quad . \tag{94}$$

The factor V_p in Equations (92) through (94) is the velocity in the flame or plume as it strikes the ceiling. It is computed from Equation (37) with the appropriate changes to account for the hot zone. The Reynolds number in Equations (92) through (94) is formed using V_p and H:

$$Re = V_p\ H/\nu \quad . \tag{95}$$

We assume that the plume impact point is always directly above the fire base center; there is no tilt due to ventilation or other influences. The distance between the plume impact point and the center of each ceiling panel is used to select among Equations (92), (93) and (94) for the value of h.

The heat transfer coefficients for the interior surfaces of the wall and floor panels are computed with the same relations as those for the exterior panel surfaces. That is, the interior surface orientation is used to select between Equations (76) and (77) for the appropriate h.

When h has been obtained for each ceiling, wall, or floor panel, the heat loss or gain per unit area of the internal surface is

$$\dot{q}''_{ci} = h\,(T - T_w) \qquad , \tag{96}$$

where T is the temperature of the zone in contact with the panel's centroid.

Equation (96) completes the forms needed to compute the four heat flux terms of Equation (74) and thus solve for the change of T_w with time for each panel.

2.10 Program Structure

The general structure of the CCFM program is fairly simple in nature, as shown by Figure 9. After reading a prepared input data file and initializing the necessary quantities, the program enters a time loop which continues until the user wishes to stop.

After each time increment, the cargo compartment's new state is computed and then reported to the user. This state consists of a set of physical quantities which appear in a coupled set of non-linear first order ordinary differential equations. The model uses the Gauss-Seidel iterative technique

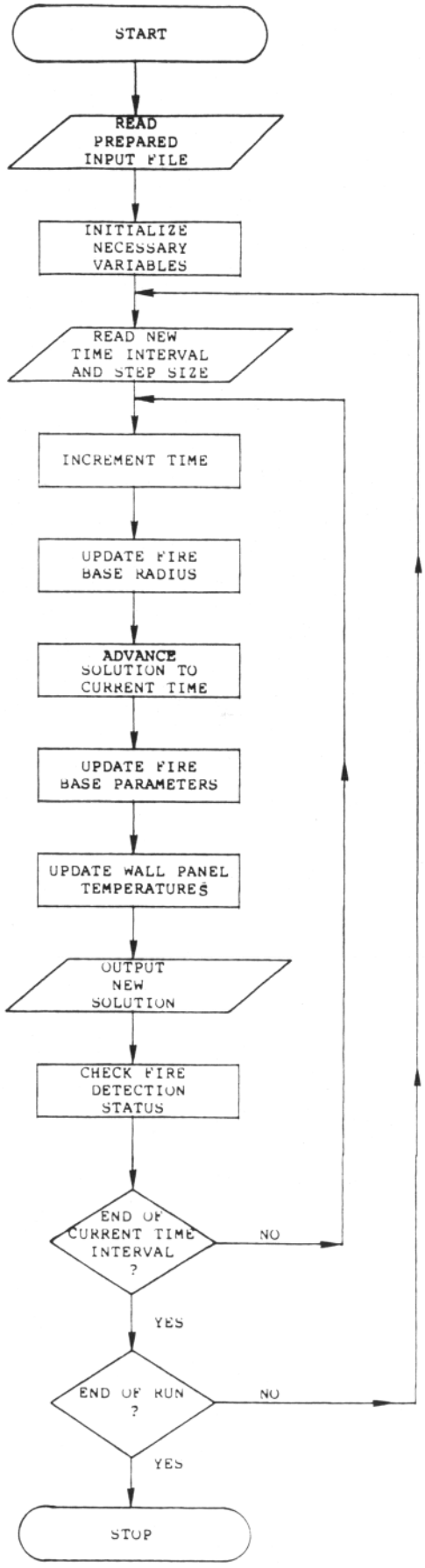

Figure 9. General Structure of the CCFM.

of successive substitution in order to compute each new solution. During each iteration, each variable in the solution set is recomputed, always making use of the most recent estimates of the other variables in the set. As soon as a variable has been recomputed, its new value immediately becomes a part of the new solution set estimate. The iterations continue until all the variables have converged (cease diverging in value) to within specified tolerances or until a maximum number of iterations has been performed. If convergence fails, the model cuts the time step size in half and makes another attempt to converge on the new solution set. If convergence fails even after the maximum number of time cuts allowed (specified in the prepared input data file), then a message is printed and the program terminates. Damping factors have been incorporated into the model in order to speed up the convergence process and to guard against divergence. The prepared input data file defines a damping factor and a convergence tolerance for each variable in the solution set.

Since the fire influences the atmospheric conditions inside the cargo compartment, its characteristics should be updated before each Gauss-Seidel iteration. Unfortunately, each fire update requires significant computation time. Therefore, in order to save time, the fire is only conditionally updated after the first iteration, based on the following criteria. This model treats the fire as two separate entities: the cool zone fire (that part of the fire inside the cool zone) and the hot zone fire (that part of the fire inside the hot zone). The cool zone fire is affected by the cool zone thickness and the density, temperature, and gas species mass fractions in the cool zone. The current values of these solution variables are compared with those values corresponding to the most recent update of the cool zone fire. If any of the relative differences is significant (greater than 10^{-3}), then both the cool zone and hot zone fire characteristics are recomputed, based on the current

solution set. Besides being a function of the cool zone fire, the hot zone fire is also influenced by the cool zone thickness and the density, temperature, and gas species mass fractions in the hot zone. If the cool zone fire characteristics do not require updating, then the current values of the above solution variables are compared with those values used during the most recent update of the hot zone fire. If any of the relative differences is significant (greater than 10^{-3}), then the hot zone fire characteristics are recomputed, based on the current solution set.

The CCFM program has been designed so that the user has interactive control over the following items. Before the simulation begins, there is an option that allows verification of the prepared input data file. Then, during the simulation, the user controls the length of each time interval and the time step size to be used during the interval. The solution computed for each time step is always displayed at the terminal (Unit 6), but interactive options also enable the user to direct these solutions to another file (Unit 8, for subsequent printing) and to generate a debug output file (Unit 7). In addition, the user can alter the areas and flow rates of the cargo compartment's vents and/or leaks throughout the course of the simulation. Finally, the user is able to stop the simulation at the end of any time interval.

Figures 10 through 21 indicate the calling arrangement for the subroutines and functions used in the CCFM program. Table I provides a brief description of each routine.

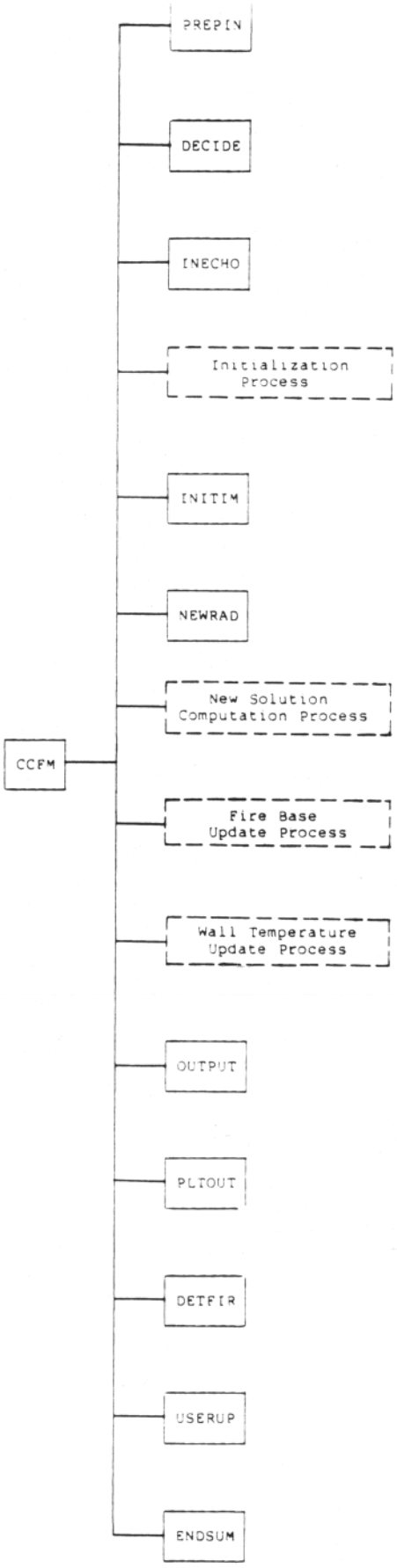

Figure 10. CCFM Main Process.

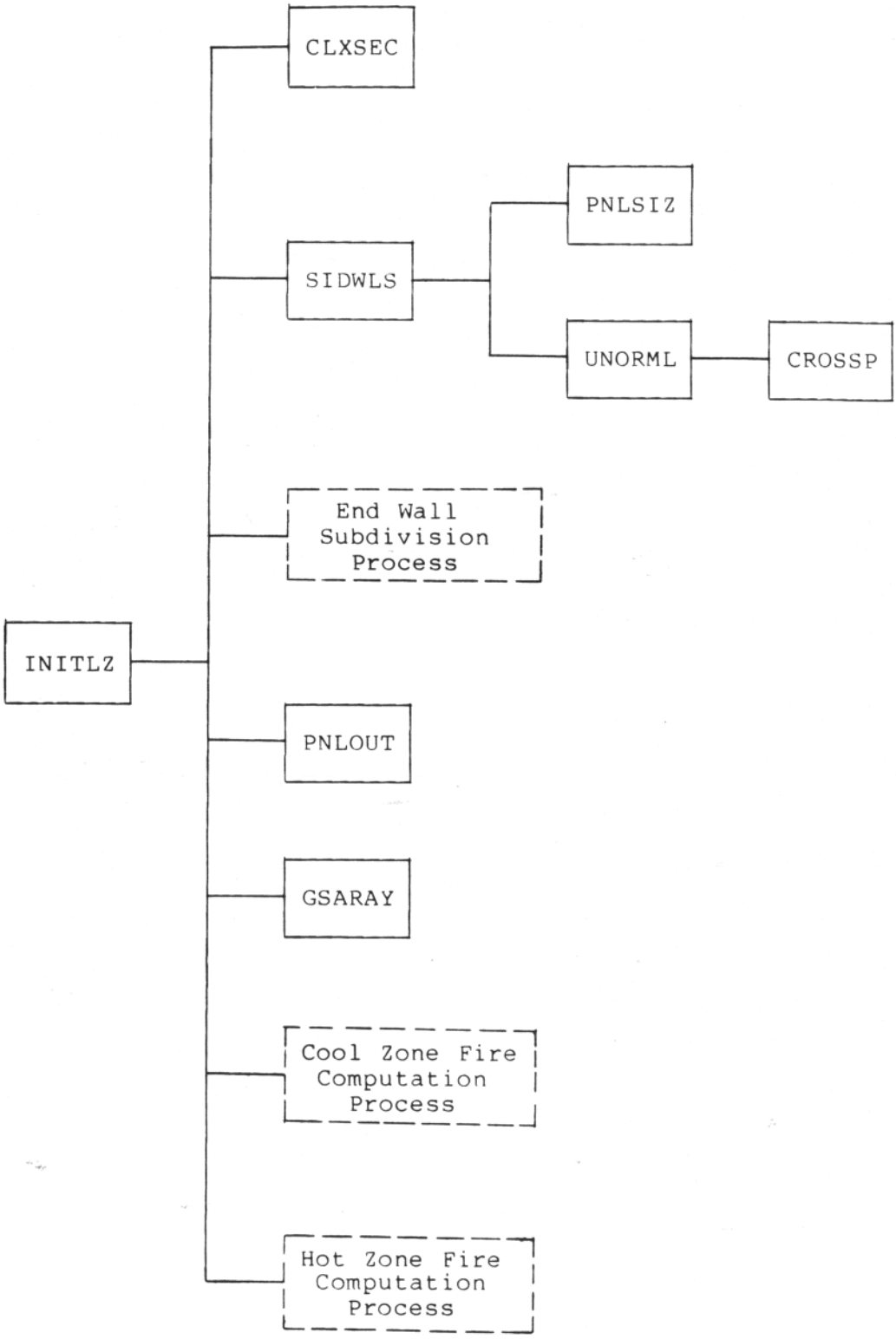

Figure 11. Initialization Process.

Figure 12. End Wall Subdivision Process.

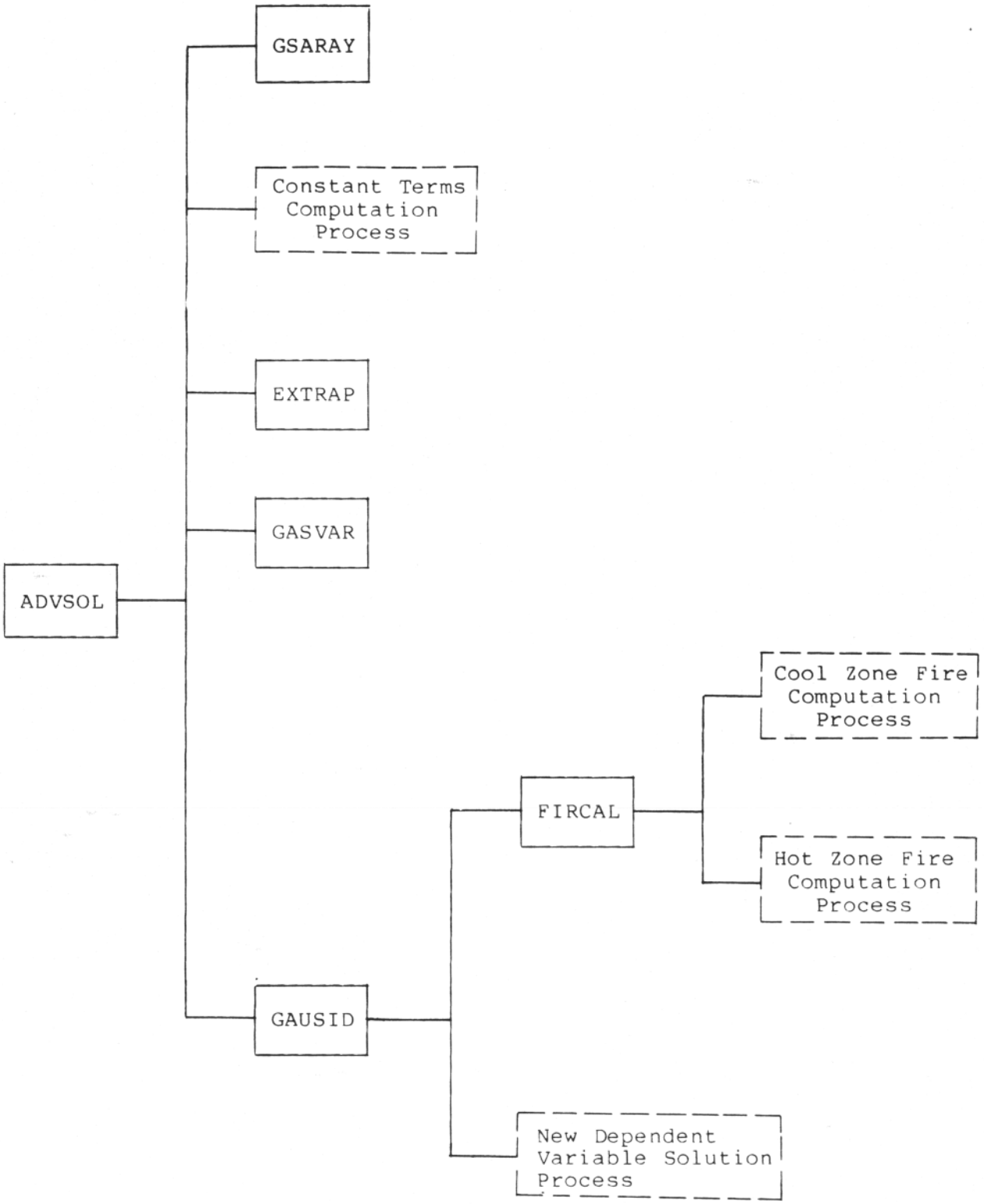

Figure 13. New Solution Computation Process.

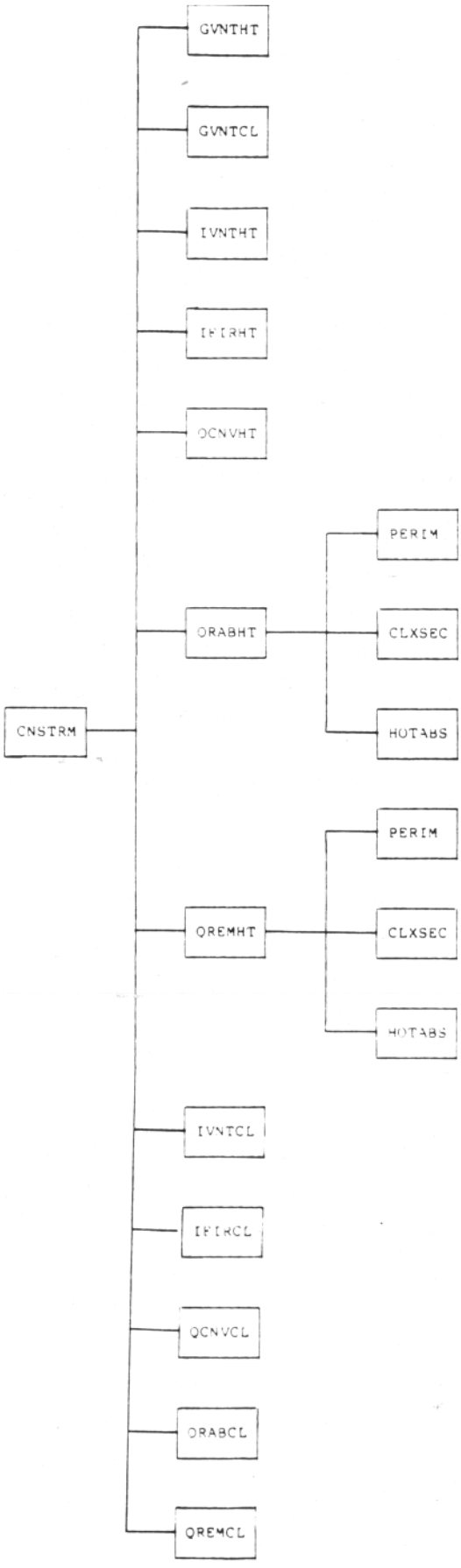

Figure 14. Constant Terms Computation Process.

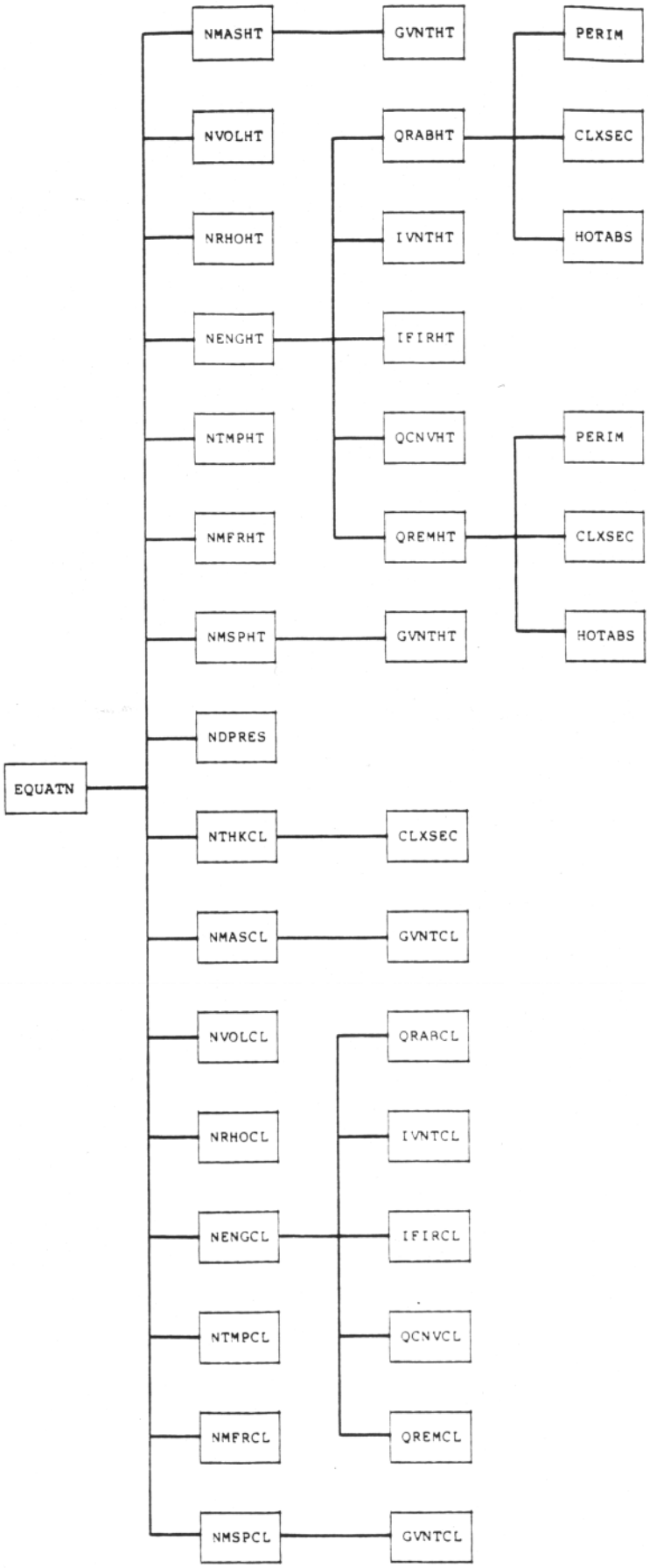

Figure 15. New Dependent Variable Solution Process.

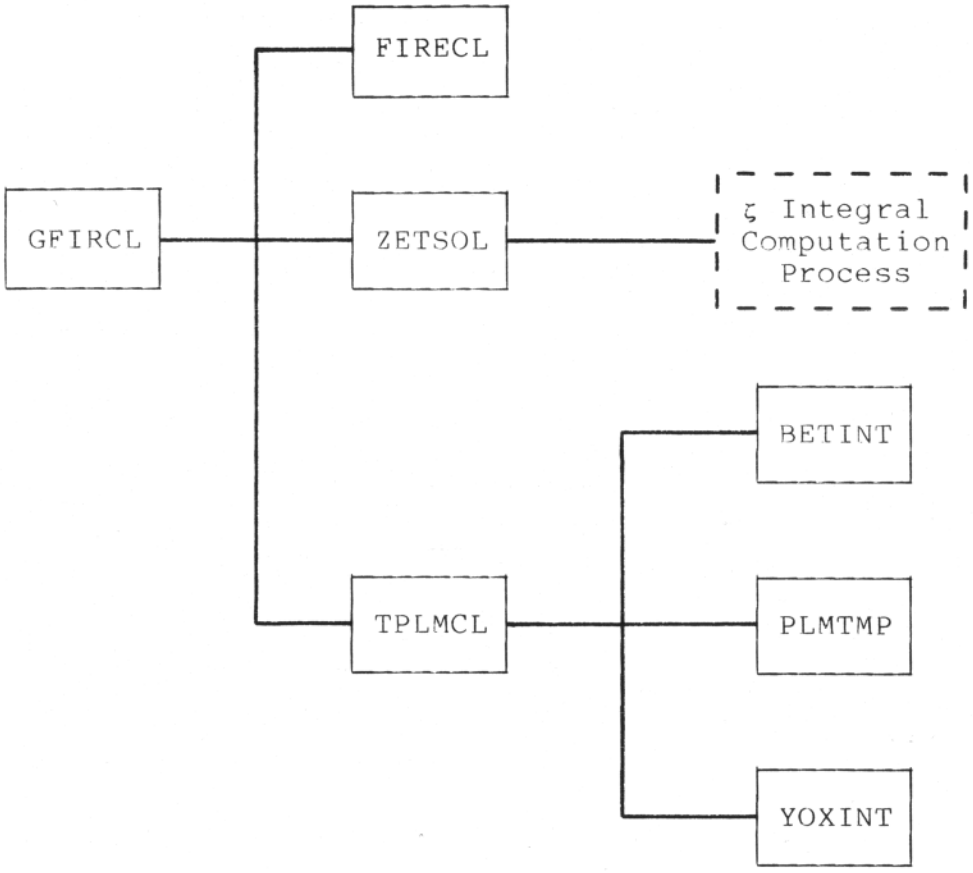

Figure 16. Cool Zone Fire Computation Process.

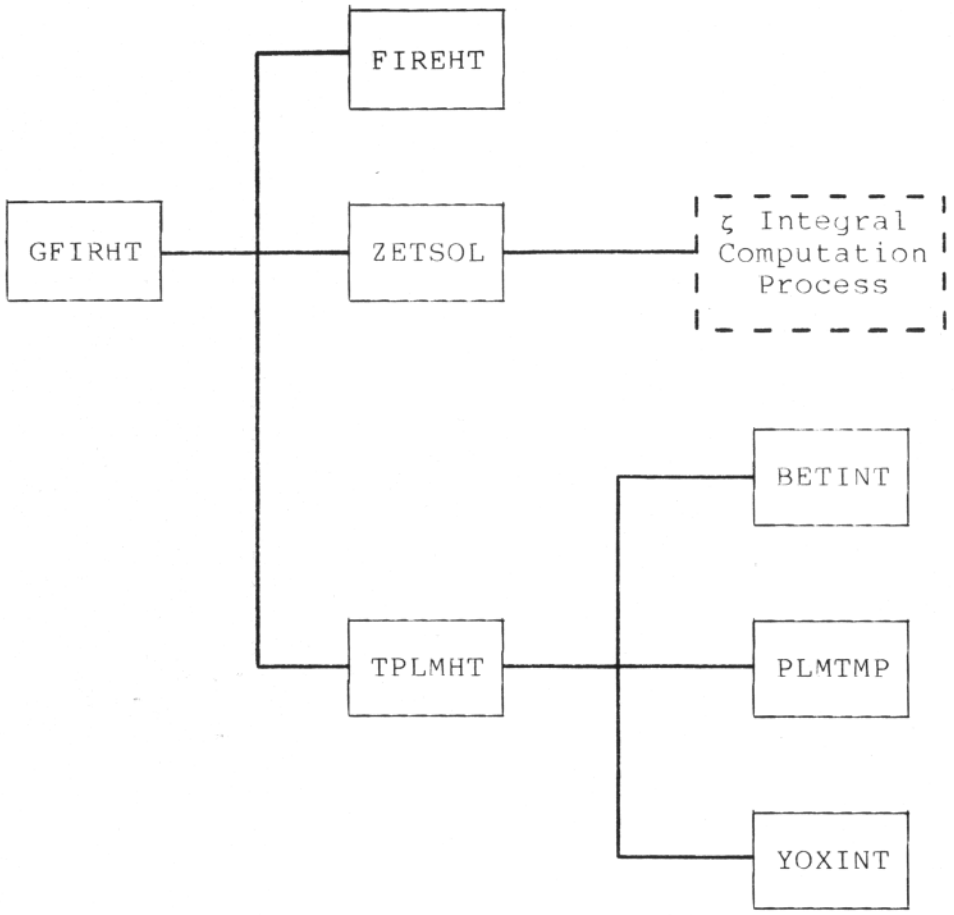

Figure 17. Hot Zone Fire Computation Process.

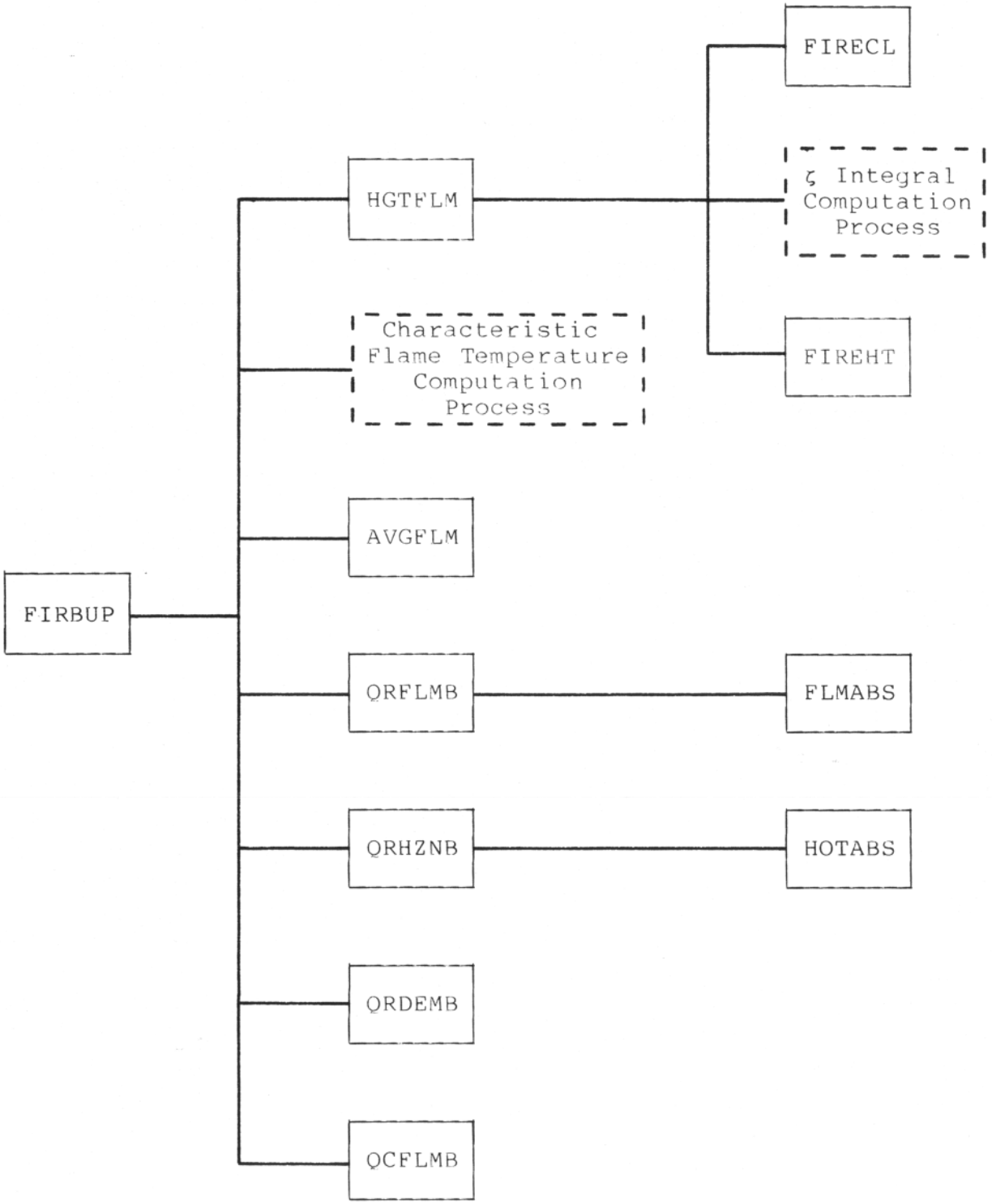

Figure 18. Fire Base Update Process.

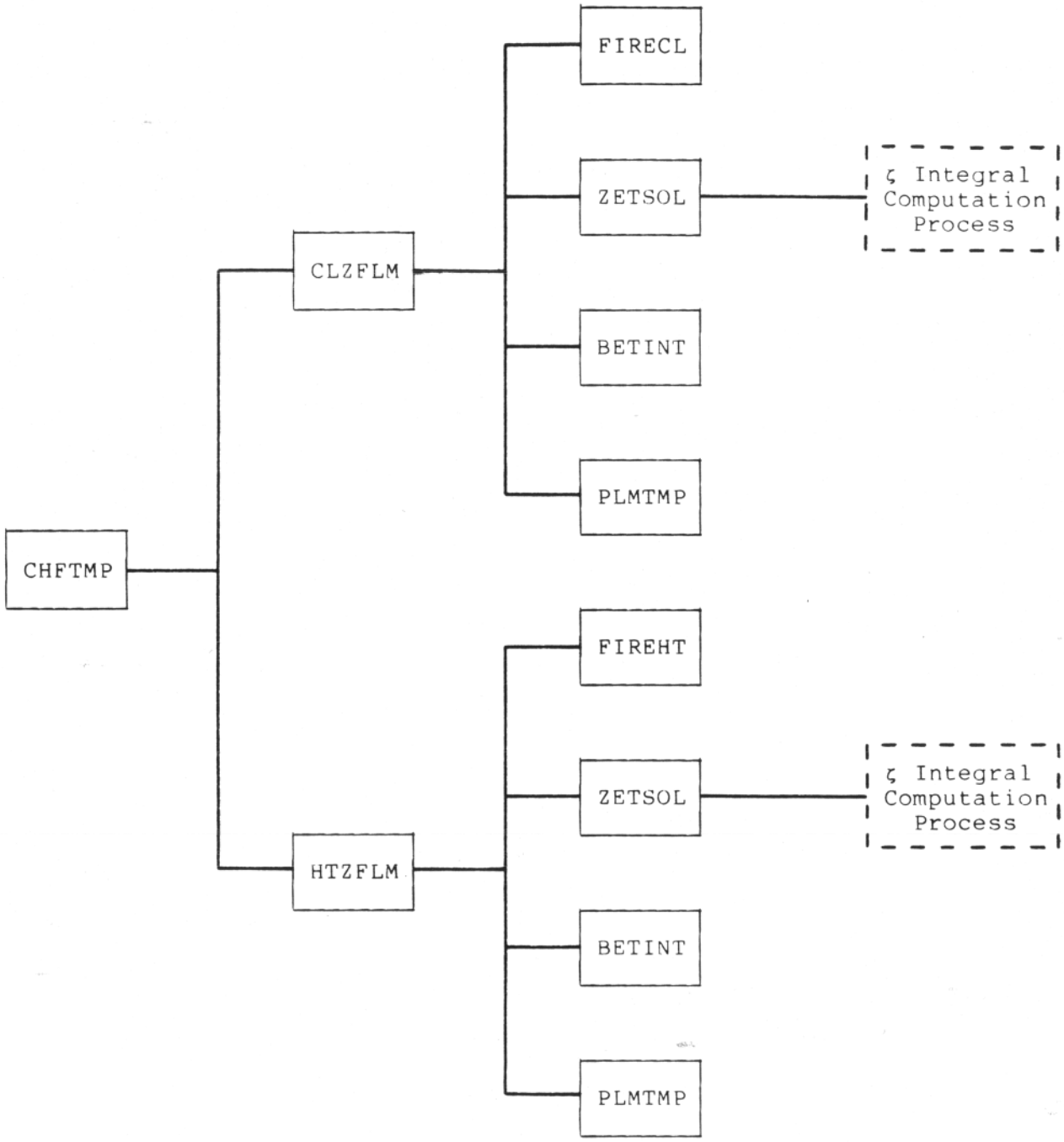

Figure 19. Characteristic Flame Temperature Computation Process.

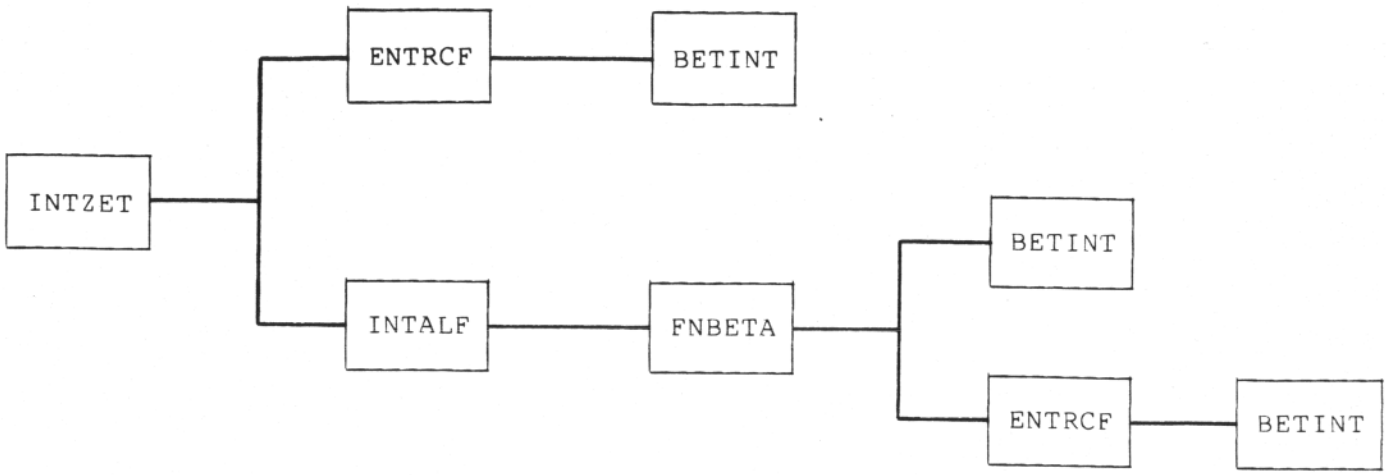

Figure 20. ζ Integral Computation Process.

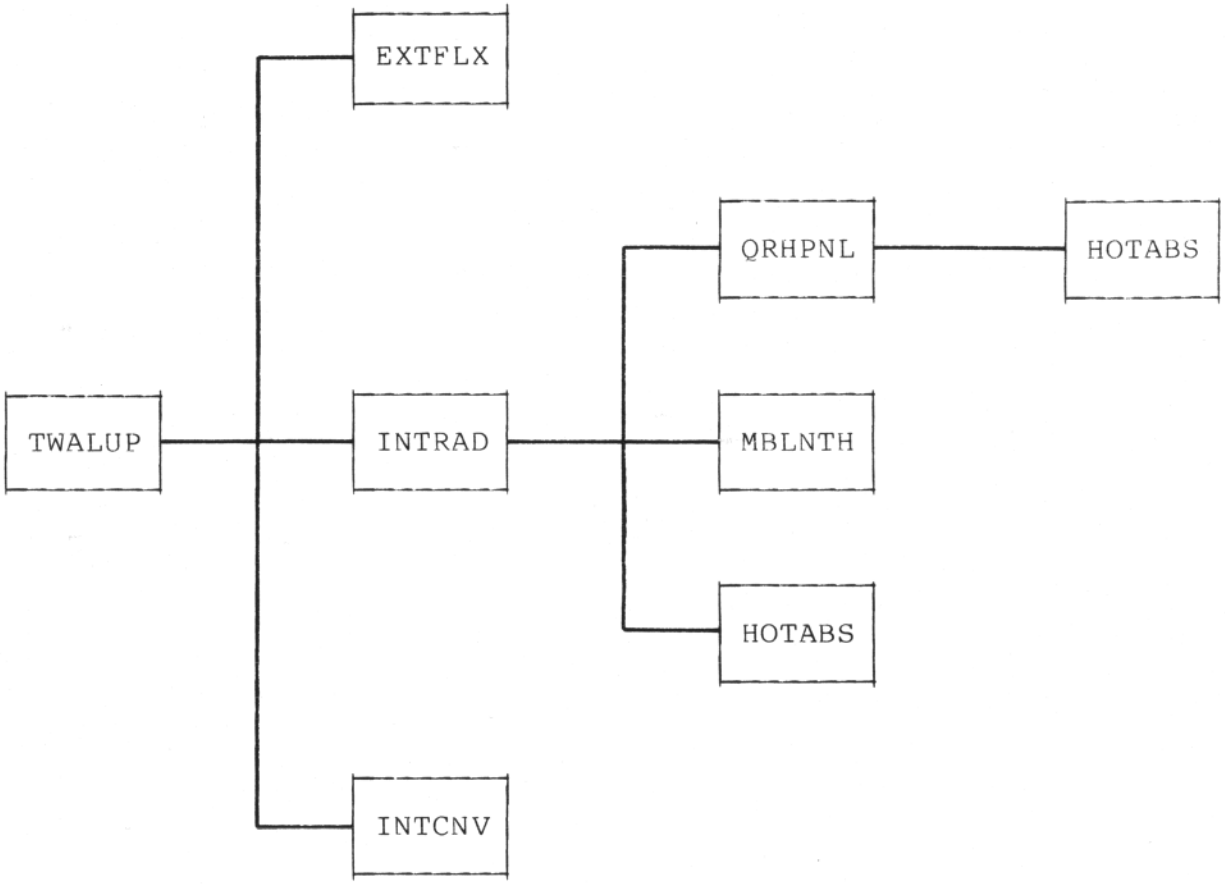

Figure 21. Wall Temperature Update Process.

TABLE I
CCFM SUBROUTINES AND FUNCTIONS

NAME	CALLED BY	FUNCTION
ADVSOL	CCFM	Controls the computation of the new solution set that describes the atmospheric conditions inside the cargo compartment
AVGFLM	FIRBUP	Averages the fire's flame height and temperature over a specified time interval
BACKWL	INITLZ	Computes and stores the centroid coordinates and a normal vector for each panel on the back end wall of the cargo compartment
BETINT	TPLMHT,FNBETA, ENTRCF,TPLMCL, CLZFLM,HTZFLM	Computes an approximation to the "beta" integral of the flame/plume calculations
BTMSID	ENDPNL	Locates the point(s) that define the bottom side of the polygon resulting from the intersection of the indicated rectangular panel with the cargo compartment's cross section
CHFTMP	FIRBUP	Computes a characteristic flame radiation temperature for the fire
CLXSEC	INITLZ,NTHKCL, QRABHT,QREMHT	Computes the cross-sectional area of the cool zone in the X-Z plane
CLZFLM	CHFTMP	Computes an average flame temperature for the part of the flame that is inside the cool zone
CNSTRM	ADVSOL	Computes and stores constant terms that are used to compute the new solution set
CROSSP	UNORML,PNTLOC, PCENTR	Computes the cross product of two vectors in 3-space
DECIDE	CCFM,INITIM, USERUP	Reads user's response to a yes/no question
DETFIR	CCFM	Determines whether or not the fire has been detected
DPRDCT	PCENTR	Computes the dot product of two vectors in 3-space

TABLE I (Continued)
CCFM SUBROUTINES AND FUNCTIONS

NAME	CALLED BY	FUNCTION
ELMDUP	ENDPNL	Eliminates all duplicate vertices defining a polygon in 3-space
ENDPNL	FRNTWL,BACKWL	Defines the vertices of the polygon resulting from the intersection of the specified rectangular panel with one of the compartment's end walls
ENDSUM	CCFM	Writes an end-of-run summary to Unit 8
ENTRCF	INTZET,FNBETA	Computes an approximate entrainment coefficient for the specified plume conditions
EQUATN	GAUSID	Controls the computation of the appropriate dependent variable in the solution set during the Gauss-Seidel iterative process
EXTFLX	TWALUP	Computes the exterior heat flux terms for the specified wall panel
EXTRAP	ADVSOL	Uses linear extrapolation technique in order to compute an initial estimate for the new solution set
FIRBUP	CCFM	Updates mass gasification rate, fuel vapor density, and fuel vapor velocity at base of the fire
FIRCAL	GAUSID	Decides when to update the fire characteristics inside the cargo compartment
FIRECL	GFIRCL,HGTFLM CLZFLM	Defines and computes the generic fire model terms to be used in the cool zone calculations for the fire
FIREHT	GFIRHT,HGTFLM HTZFLM	Defines and computes the generic fire model terms to be used in the hot zone calculations for the fire
FLMABS	QRFLMB	Computes an approximate flame absorption coefficient
FNBETA	INTALF	Computes the integrand for the integral evaluated in subroutine INTALF

TABLE I (Continued)
CCFM SUBROUTINES AND FUNCTIONS

NAME	CALLED BY	FUNCTION
FRNTWL	INITLZ	Computes and stores the centroid coordinates and a normal vector for each panel on the front end wall of the cargo compartment
GASVAR	ADVSOL	Transfers the extrapolated solution estimate from a local array to the corresponding global variables
GAUSID	ADVSOL	Uses Gauss-Seidel technique to converge on new gas solution set
GFIRCL	INITLZ,FIRCAL	Computes the total mass flow rate of gas from the cool zone into the fire
GFIRHT	INITLZ,FIRCAL	Computes the total mass flow rates of gas between the hot zone and the fire
GSARAY	INITLZ,ADVSOL	Transfers the current gas solution set from global variables (in a common block) to a local array
GVNTCL	CNSTRM,NMASCL, NMSPCL	Computes net mass flow rate of gas into and out of cool zone through vents and leaks
GVNTHT	CNSTRM,NMASHT, NMSPHT	Computes net mass flow rate of gas into and out of hot zone through vents and leaks
HGTFLM	FIRBUP	Computes the flame height for the fire
HOTABS	INTRAD,QRABHT, QREMHT,QRHPNL, QRHZNB	Computes the hot zone absorption coefficient
HRZINT	TOPSID,BTMSID	Computes the intersection (if any) of a horizontal line segment (in the X-Z plane) with one of the line segments defining the compartment's cross section
HTZFLM	CHFTMP	Computes an average flame temperature for the part of the flame that is inside the hot zone
IFIRCL	CNSTRM,NENGCL	Computes the enthalpy flow rate due to the mass flow of gas from the cool zone into the fire
IFIRHT	CNSTRM,NENGHT	Computes the enthalpy flow rates due to the mass flow of gas between the hot zone and the fire

TABLE I (Continued)
CCFM SUBROUTINES AND FUNCTIONS

NAME	CALLED BY	FUNCTION
INECHO	CCFM	Echoes the prepared input data file so that the user can verify the input
INITIM	CCFM	Reads the initial time interval and step size for the simulation
INITLZ	CCFM	Initializes necessary variables before the simulation can begin
INTALF	INTZET	Computes numerical solution for integral that appears in the integrand expression for the integral evaluated in subroutine INTZET
INTCNV	TWALUP	Computes the interior surface convection heat flux term for the specified wall panel
INTRAD	TWALUP	Computes the interior surface radiation heat flux term for the specified wall panel
INTZET	ZETSOL,HGTFLM	Computes numerical solution for integral involved in plume mass flow ratio computation
IVNTCL	CNSTRM,NENGCL	Computes net enthalpy flow rate due to mass flow of gas into and out of cool zone through vents and leaks
IVNTHT	CNSTRM,NENGHT	Computes net enthalpy flow rate due to mass flow of gas into and out of hot zone through vents and leaks
LFTSID	ENDPNL	Locates the point(s) that define the left side of the polygon resulting from the intersection of the indicated rectangular panel with the cargo compartment's cross section
MBLNTH	INTRAD	Computes the four mean beam lengths for the specified wall panel in contact with the hot zone
NDPRES	EQUATN	Computes a new estimate for the cargo compartment's interior-exterior pressure difference
NENGCL	EQUATN	Computes a new estimate for the enthalpy of the cool zone

TABLE I (Continued)
CCFM SUBROUTINES AND FUNCTIONS

NAME	CALLED BY	FUNCTION
NENGHT	EQUATN	Computes a new estimate for the enthalpy of the hot zone
NEWRAD	CCFM	Updates the radius and surface area of the fire base inside the cargo compartment
NMASCL	EQUATN	Computes a new estimate for the total mass of gas in the cool zone
NMASHT	EQUATN	Computes a new estimate for the total mass of gas in the hot zone
NMFRCL	EQUATN	Computes a new estimate for the mass fraction of the specified gas species in the cool zone
NMFRHT	EQUATN	Computes a new estimate for the mass fraction of the specified gas species in the hot zone
NMSPCL	EQUATN	Computes a new estimate for the mass of the specified gas species in the cool zone
NMSPHT	EQUATN	Computes a new estimate for the mass of the specified gas species in the hot zone
NRHOCL	EQUATN	Computes a new estimate for the cool zone density
NRHOHT	EQUATN	Computes a new estimate for the hot zone density
NTHKCL	EQUATN	Computes a new estimate for the cool zone "thickness" (z coordinate of cool zone/hot zone interface)
NTMPCL	EQUATN	Computes a new estimate for the cool zone temperature
NTMPHT	EQUATN	Computes a new estimate for the hot zone temperature
NVOLCL	EQUATN	Computes a new estimate for the cool zone volume
NVOLHT	EQUATN	Computes a new estimate for the hot zone volume
OUTPUT	CCFM	Prints the new solution set

TABLE I (Continued)
CCFM SUBROUTINES AND FUNCTIONS

NAME	CALLED BY	FUNCTION
PCENTR	FRNTWL,BACKWL	Computes the surface area and centroid coordinates of a convex polygon in 3-space
PERIM	QRABHT,QREMHT	Computes the perimeter length in the X-Z plane formed by the contact of the cool zone with the compartment walls
PLMTMP	TPLMHT,TPLMCL, CLZFLM,HTZFLM	Computes the temperature at the specified location in the plume
PLTOUT	CCFM	Writes information to a file for subsequent plotting
PNLOUT	INITLZ	Writes out (to Unit 8) the location, orientation, and size of each compartment wall panel
PNLSIZ	SIDWLS,FRNTWL, BACKWL	Determines the "optimum" grid and panel size for the indicated rectangular wall
PNTLOC	ENDPNL,LFTSID, TOPSID,RGTSID, BTMSID	Determines if a point is inside or outside the bounds of the convex polygon defining the cargo compartment's cross section
PREPIN	CCFM	Reads the user's prepared input data file
QCFLMB	FIRBUP	Computes the flame-to-base convective heat flux for the specified fire
QCNVCL	CNSTRM,NENGCL	Computes the convective heat transfer rate between compartment surfaces and cool zone gases
QCNVHT	CNSTRM,NENGHT	Computes the convective heat transfer rate between compartment surfaces and hot zone gases
QRABCL	CNSTRM,NENGCL	Computes radiation absorption rate for cool zone
QRABHT	CNSTRM,NENGHT	Computes radiation absorption rate for hot zone
QRDEMB	FIRBUP	Computes the radiation flux emitted from the fire base surface
QREMCL	CNSTRM,NENGCL	Computes a radiation emission rate for the cool zone

TABLE I (Continued)
CCFM SUBROUTINES AND FUNCTIONS

NAME	CALLED BY	FUNCTION
QREMHT	CNSTRM,NENGHT	Computes a radiation emission rate for the hot zone
QRFLMB	FIRBUP	Computes the average flame-to-base radiant heat flux for the fire
QRHPNL	INTRAD	Computes the radiant heat flux from the hot zone to the surface of the specified wall panel in contact with the cool zone
QRHZNB	FIRBUP	Computes the radiant heat flux from the hot zone to the base of the fire
RGTSID	ENDPNL	Locates the point(s) that define the right side of the polygon resulting from the intersection of the indicated rectangular panel with the cargo compartment's cross section
SIDWLS	INITLZ	Computes and stores the centroid coordinates and a normal vector for each panel on the side walls of the cargo compartment
TOPSID	ENDPNL	Locates the point(s) that define the top side of the polygon resulting from the intersection of the indicated rectangular panel with the cargo compartment's cross section
TPLMCL	GFIRCL	Computes the plume characteristics at the top of the cool zone (interface between cool and hot zones) for the fire
TPLMHT	GFIRHT	Computes the plume characteristics at the top of the hot zone (compartment ceiling) for the fire
TWALUP	CCFM	Updates the cargo compartment's wall panel temperatures
UNORML	SIDWLS	Computes the unit normal vector for the specified convex polygon in 3-space
USERUP	CCFM	Reads new time interval and step size for simulation

TABLE I (Concluded)
CCFM SUBROUTINES AND FUNCTIONS

NAME	CALLED BY	FUNCTION
VRTINT	LFTSID,RGTSID	Computes the intersection (if any) of a vertical line segment (in the X-Z plane) with one of the line segments defining the compartment's cross section
YOXINT	TPLMHT,TPLMCL	Computes integral approximation used to calculate the oxygen mass fraction inside a plume
ZETSOL	GFIRHT,GFIRCL, CLZFLM,HTZFLM	Computes the plume mass flow ratio for the fire inside either the hot or cool zone

SECTION 3
SAMPLE RESULTS

This section presents the results of a sample run of the CCFM for a typical cargo compartment fire situation. The test case has been chosen to illustrate the main features and operation of the model, but, being only a single case, does not illustrate many of the options available. The situation is a fire on a slab of polyurethane foam located near the floor of a compartment of about 10 m^3 in volume. Forced air ventilation enters through an inflow vent near the floor of one wall and exits through an outflow vent located at the same point on the opposite wall. The test case was run for ten minutes of simulated time and illustrates the effect of the hot zone development upon the burning rate.

3.1 INPUT DATA

Table II summarizes the input for this sample test case. The cargo compartment is a rectangular volume 2.34 x 2.73 x 1.52 meters (7.68 x 8.96 x 5.00 feet). Total volume is 9.71 cubic meters (344 cubic feet). The fire is taken to be located near the floor at 0.1 meters (0.33 feet) above it. The fire base is assumed to be a circle of diameter of 0.364 meters (1.2 feet) on a horizontally upward facing slab of polyurethane foam. There is no load in the compartment. The situation is shown schematically in Figure 22.

Ventilation is provided through the forced flow inflow vent and a free flow exhaust vent, both located at 0.1 meters (0.33 feet) above the floor. Both vent areas are 1.82 x 10^{-2} m^2 (1.96 x 10^{-1} ft^2) in area which is equivalent to a circle of six inches in diameter. The flow rate through the inflow vent is fixed throughout the simulation as 6.14 x 10^{-2} m^3/s

(130 ft^3/min). The pressure outside the compartment is taken to be one atmosphere (1.013×10^5 Pa) and the pressure inside is taken to be 15 Pa above the ambient due to the effect of the forced inflow. The initial temperature of the compartment is 300°K (80°F) and the composition of the air is 21% oxygen and 79% nitrogen by volume (0.23 and 0.77 mass fraction).

To simulate the development of the fire, we have used a ramp function to compute the base radius as a function of time. At time 0 the radius is 0.01 meters and it increases linearly to 0.182 meters at 15 seconds. Thereafter it remains at 0.182 meters throughout the simulation. We assume that there is sufficient fuel available so that the fire would burn steadily, given enough oxygen, throughout the entire time period. All the descriptive quantities of the fuel shown in Table II are taken from the best available data for generic polyurethane foam. Most of the data comes from the work of Tewarson [Ref. 18]. The stoichiometric coefficients for the reaction are obtained assuming the following one step combustion reaction for polyurethane foam:

(97) $CH_{1.91}O_{0.263} + 0.943O_2 \rightarrow 0.7CO2 + 0.67H_2O + 0.3(CH_{1.91}O_{0.263})$

Note that the reaction does not assume complete combustion. Some of the fuel is assumed to go unburned and appears as smoke whose mean molecular weight is the same as the original fuel.

Each of the six walls of the compartment is divided into sixteen panels as shown in Table II. The ceiling and side walls are assumed to be 7.620×10^{-4} m (0.030 inch) thick. Since no data could be found on the specific fiber reinforced polymers used in cargo compartments, the values for the specific heat and density of the wall and ceiling materials were taken from Reference [19] as those of natural rubber. For the floor we assumed the material to be steel sheet of 2.54×10^{-3} m (0.100 inch) thickness; the specific heat and density are taken from Reference [19] as typical of that material.

With the exception of the first five seconds of the simulation, a time step of one second was chosen and a total time of 600 seconds (10 minutes) was run. During the first five seconds the step size was 0.5 seconds in order to better handle the rapid changes at the start. All variables except the interior/exterior pressure difference were required to converge to within one part in 10^5. No tolerance was placed on the interior/exterior pressure difference.

3.2 RESULTS

Results of the test case are shown in Figures 23 through 31. Figure 23 shows the position of the hot zone/cool zone interface (cool zone thickness) as a function of time. Starting at the ceiling, the boundary between the two zones drops quickly for about the first 100 seconds and then, as more of the fire is covered by the hot zone, its rate of movement slows until it is moving very slowly at the end of 10 minutes. This is due to the progressively smaller amount of air that is entrained from the cool zone as the flame and plume column is encompassed by the hot zone.

In Figure 24, the temperatures of the hot and cool zone are shown. The hot zone temperature rises quickly, reaching a maximum of approximately 335 K (143°F) by 240 seconds. The cool zone temperature also rises due to the effect of compression by the hot zone and heating from the lower surfaces. After a moderate rise through 180 seconds, it heats slowly throughout the rest of the simulation.

In Figure 25 the mass fraction of oxygen in the hot zone drops from its initial value of 0.23 at time 0 to just slightly above 0.18 at the end of 10 minutes. The concentration of combustion products in the hot zone is shown in Figure 26. The mass fraction of CO_2 rises steadily until it reaches 0.044 at the end

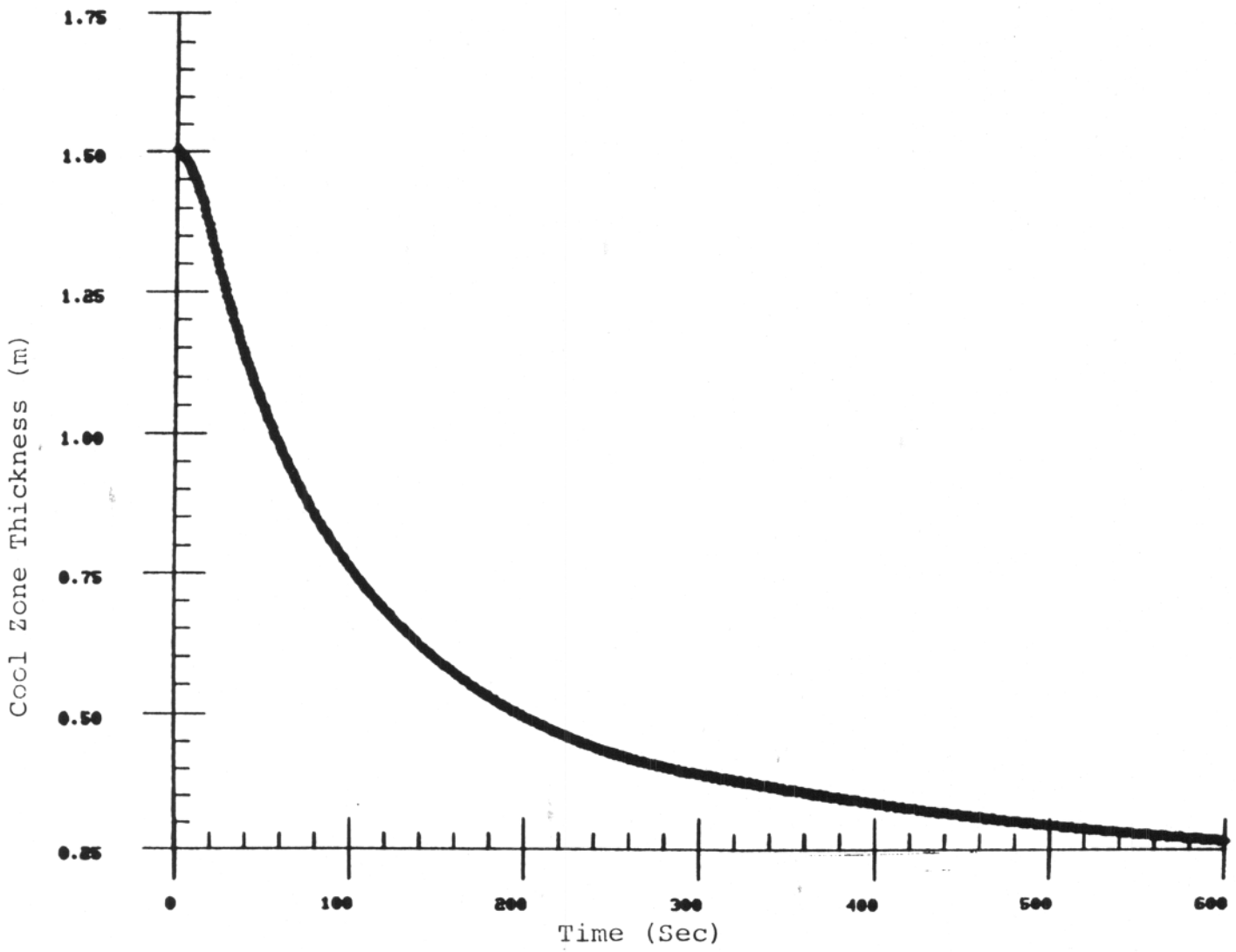

Figure 23. Cool Zone Thickness.

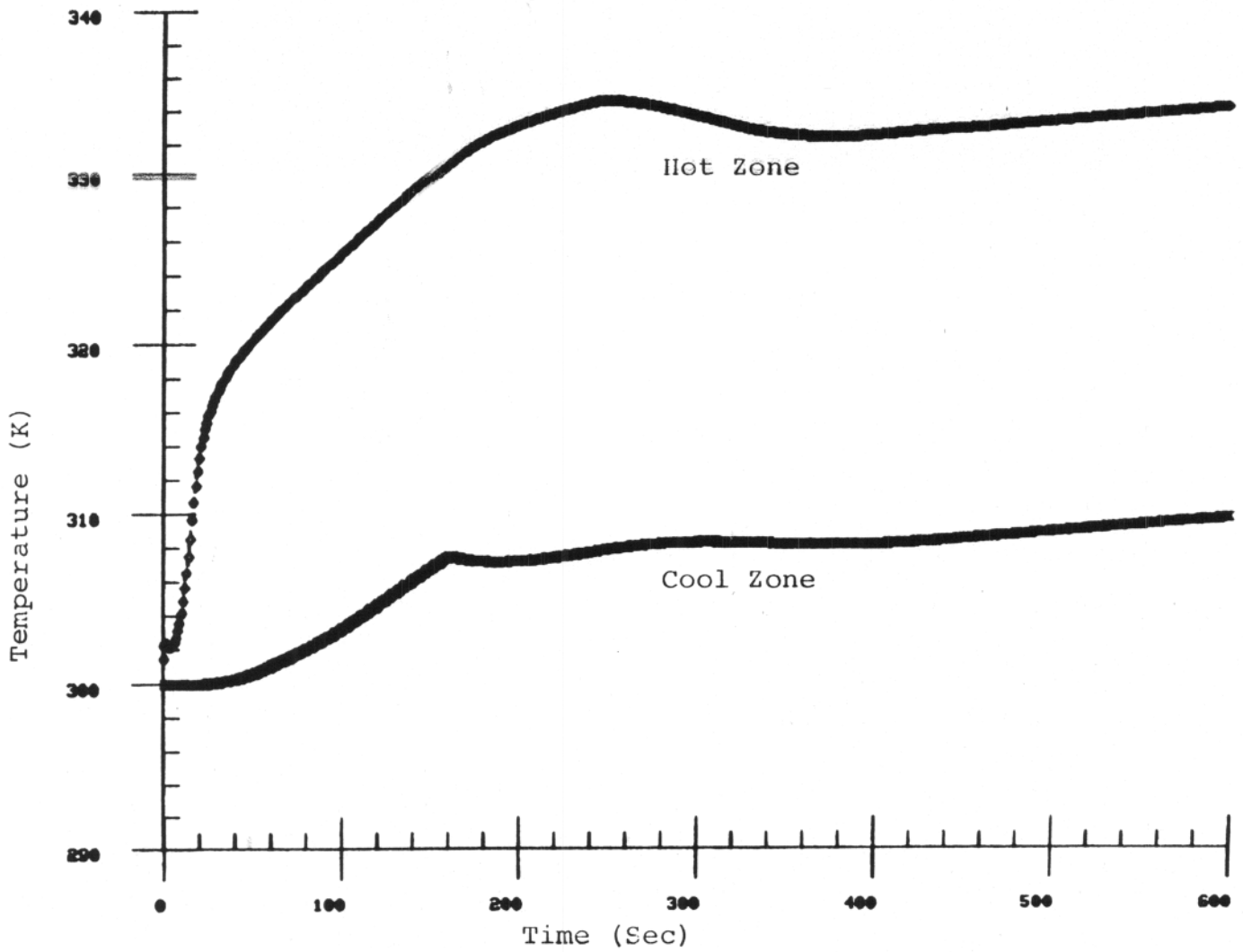

Figure 24. Zone Temperatures.

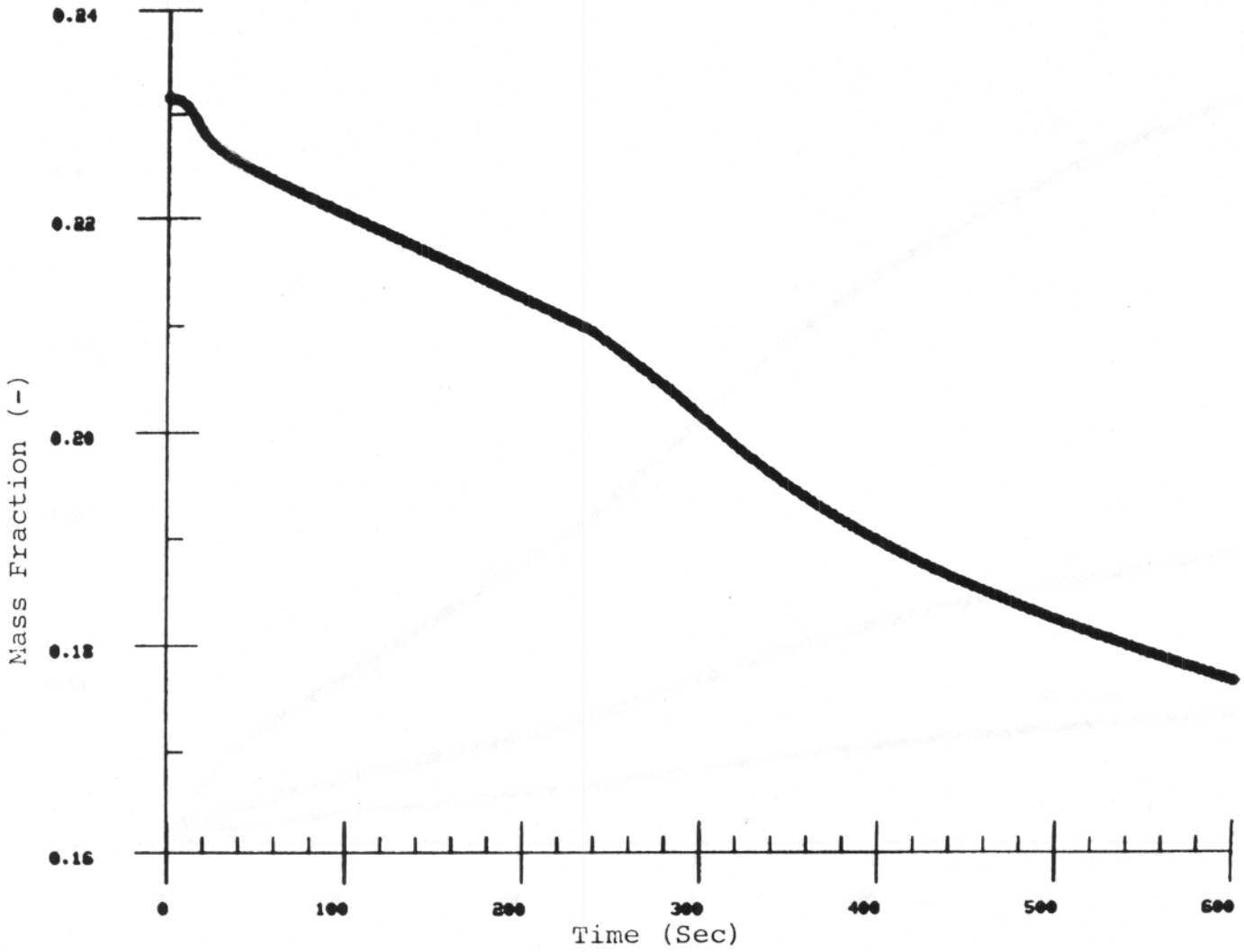

Figure 25. Hot Zone Oxygen Mass Fraction.

of 10 minutes. In a similar fashion the mass fractions of water and of the "smoke material" reach values of 0.017 and 0.0078 respectively at the end of the simulation.

Figure 27 presents the interior/exterior pressure difference throughout the 10 minutes. The oscillating values at each succeeding half second time step are the result of not forcing this quantity to converge to a small tolerance. However, we see that the calculations seem to center about a reasonably well-defined average which appears to start out at approximately 17 Pa (2.47×10^{-3} psi), drop slowly to about 15 Pa (2.18×10^{-3} psi) and remain at that value until the end of the run. It should be noted that the average magnitude of the difference in pressure is only 0.015% of the total interior pressure and, therefore, the oscillations have a negligible effect upon those variables that are functions of the total pressure, in particular the zone temperatures.

Figure 28 shows the flame height of the fire which, after making a very short dip prior to 10 seconds, rises to a steady value of approximately 0.32 meters (1.05 ft.) between 20 seconds and 250 seconds. At 250 seconds the hot zone reaches the flame tip and, as it moves over the tip, the oscillations in the flame height occur due to the lengthening of that part of the flame which enters the hot zone. The resultant decrease in the heat feedback to the fuel decreases the fuel vaporization rate. When the vaporization rate drops, the flame height drops, and for the period between 250 and about 320 seconds, the flame tip oscillates in and out of the hot zone. Beyond 320 seconds the zone has moved down far enough so that the flame tip stays within the hot zone at each step. Figure 29 shows the flame absorption coefficient remaining constant at 1.62 m^{-1} until the flame penetrates the hot zone. The effect of the decreased oxygen in the hot zone then lowers the value. The decline has reached almost exactly 1.0 m^{-1} at the end of the run.

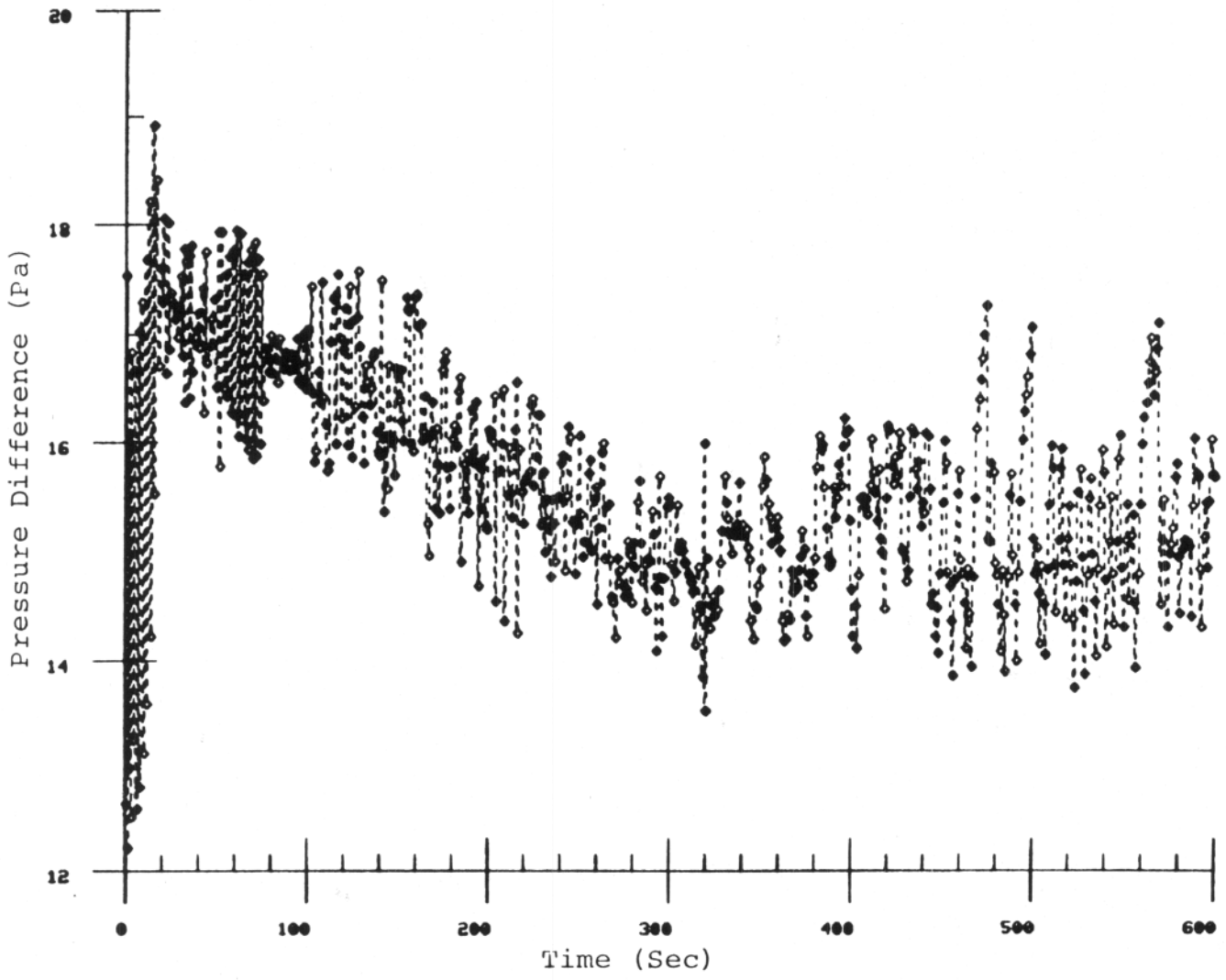

Figure 27. Pressure Difference Between the Interior and Exterior.

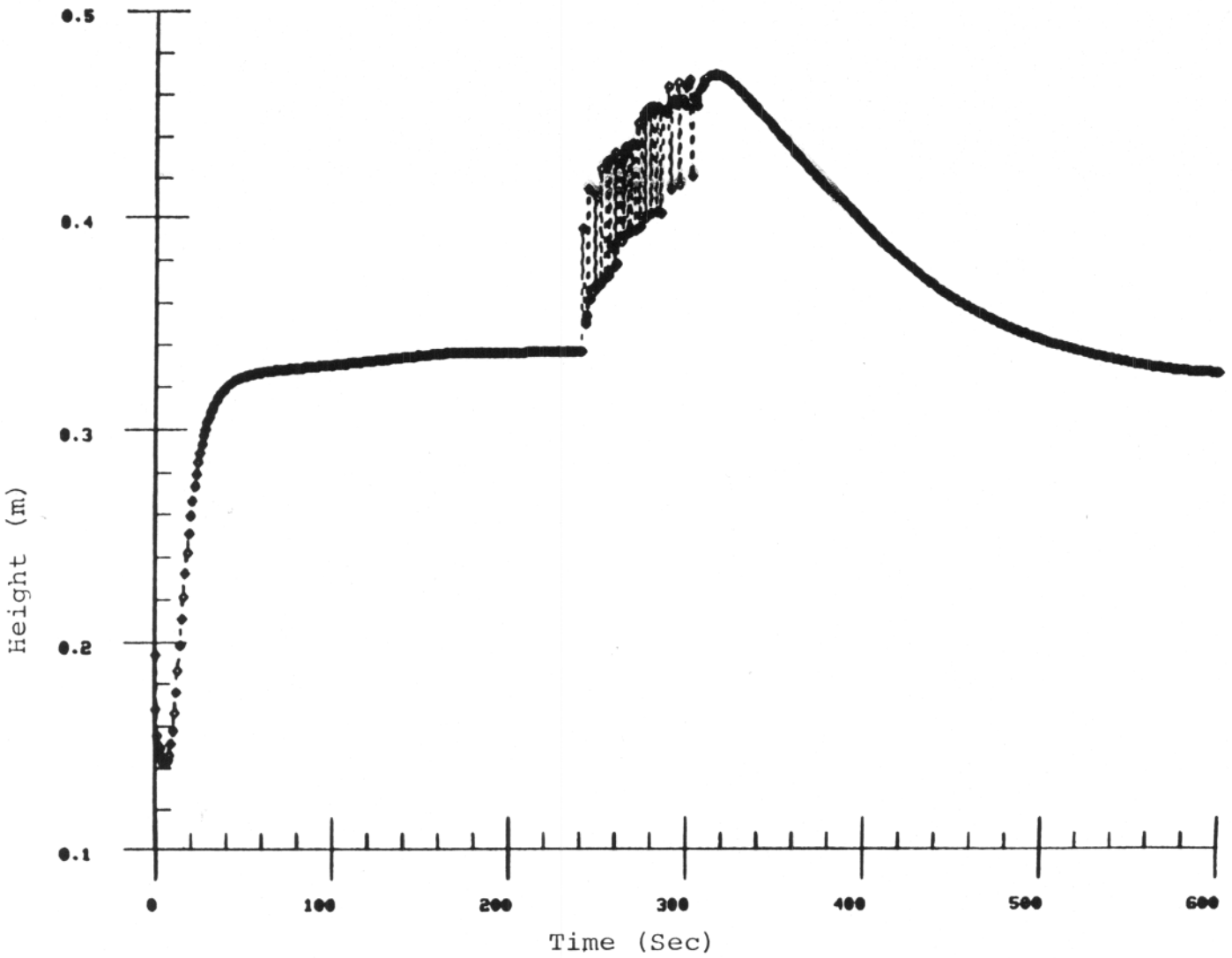

Figure 28. Flame Height.

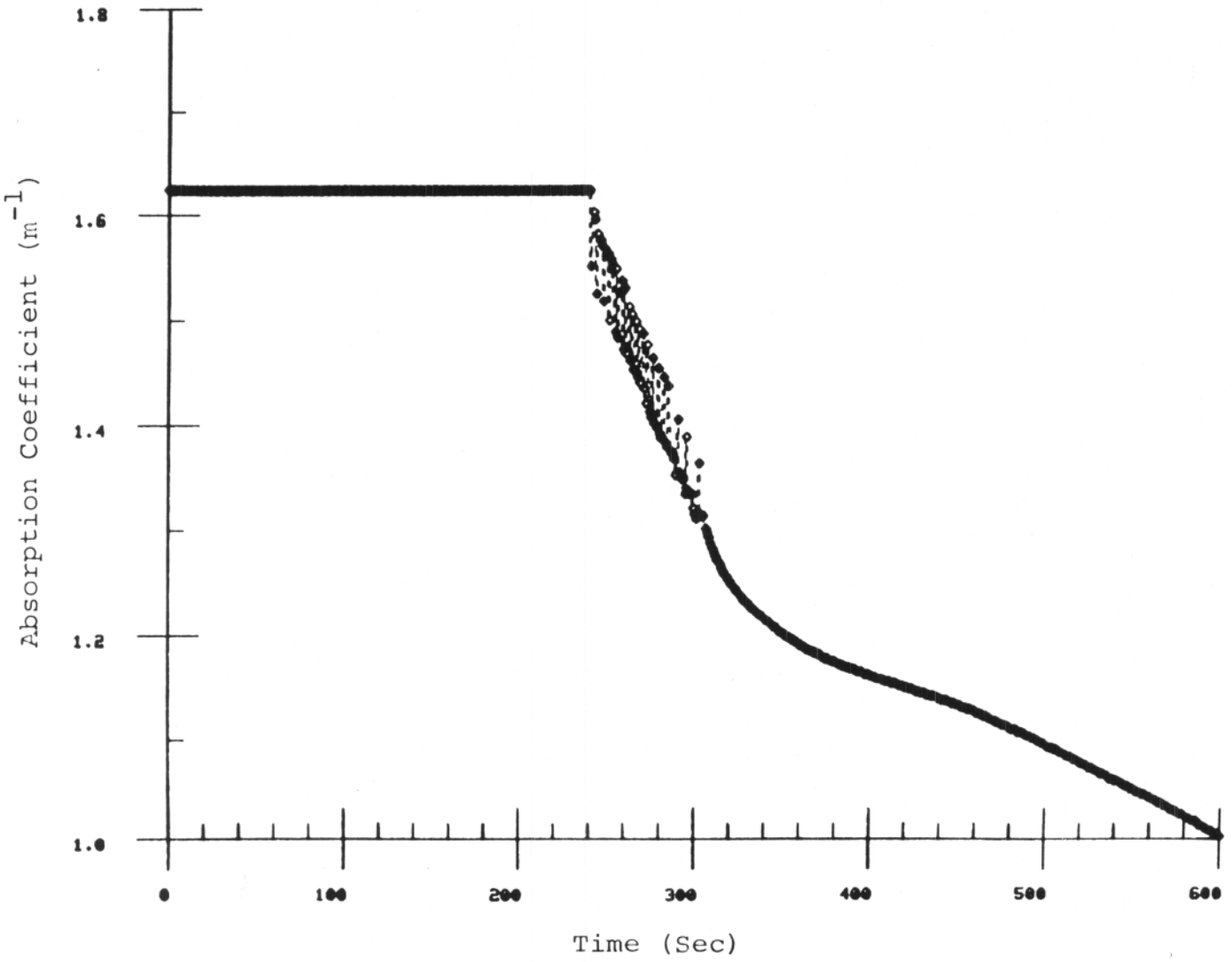

Figure 29. Flame Absorption Coefficient.

Figure 30 gives the average flame temperature as a function of time. We see that the value remains approximately steady at 1150 K (1610°F) until the flame penetrates the hot zone. After this time, the temperature drops quickly through an oscillating region caused by the instability effects explained above. After breaking out of the oscillation region, the flame temperature reaches a minimum of about 970 K (1286°F) near 320 seconds and then rises once again on a somewhat uneven course until it is approximately 1080 K (1484°F) at 10 minutes. The cause of the rise after 320 seconds is apparently due to the increasing amount of hot gas entrained into the combustion area of the flame resulting in an increase in the average flame temperature.

We see in Figures 29 and 30 the effects of two counteracting influences on the burning rate. The flame absorption coefficient, which partially determines the radiant output of the flame, drops monotonically as less oxygen is available to the fire. On the other hand, since the fire can entrain: (1) gas of a progressively higher temperature, and (2) progressively more of this gas as the hot zone moves down, the flame temperature, which also appears in the radiation expression, increases.

In Figure 31 the result of these two counteracting influences on the burning rate (as measured by the mass gasification rate) is evident. After an initial quick rise to the value of approximately 0.32×10^{-3} kg/s (0.7×10^{-3} lbm/s), the rate remains rather constant until the hot zone reaches the flame tip. Between 250 seconds and approximately 320 seconds, the burning rate declines due primarily to the change in the absorption coefficient and flame temperatue as the flame is established in the hot zone. However, after 320 seconds, the effects of the rising flame temperature and decreasing absorption coefficient seem to offset, and the burning rate fluctuates about an approximately

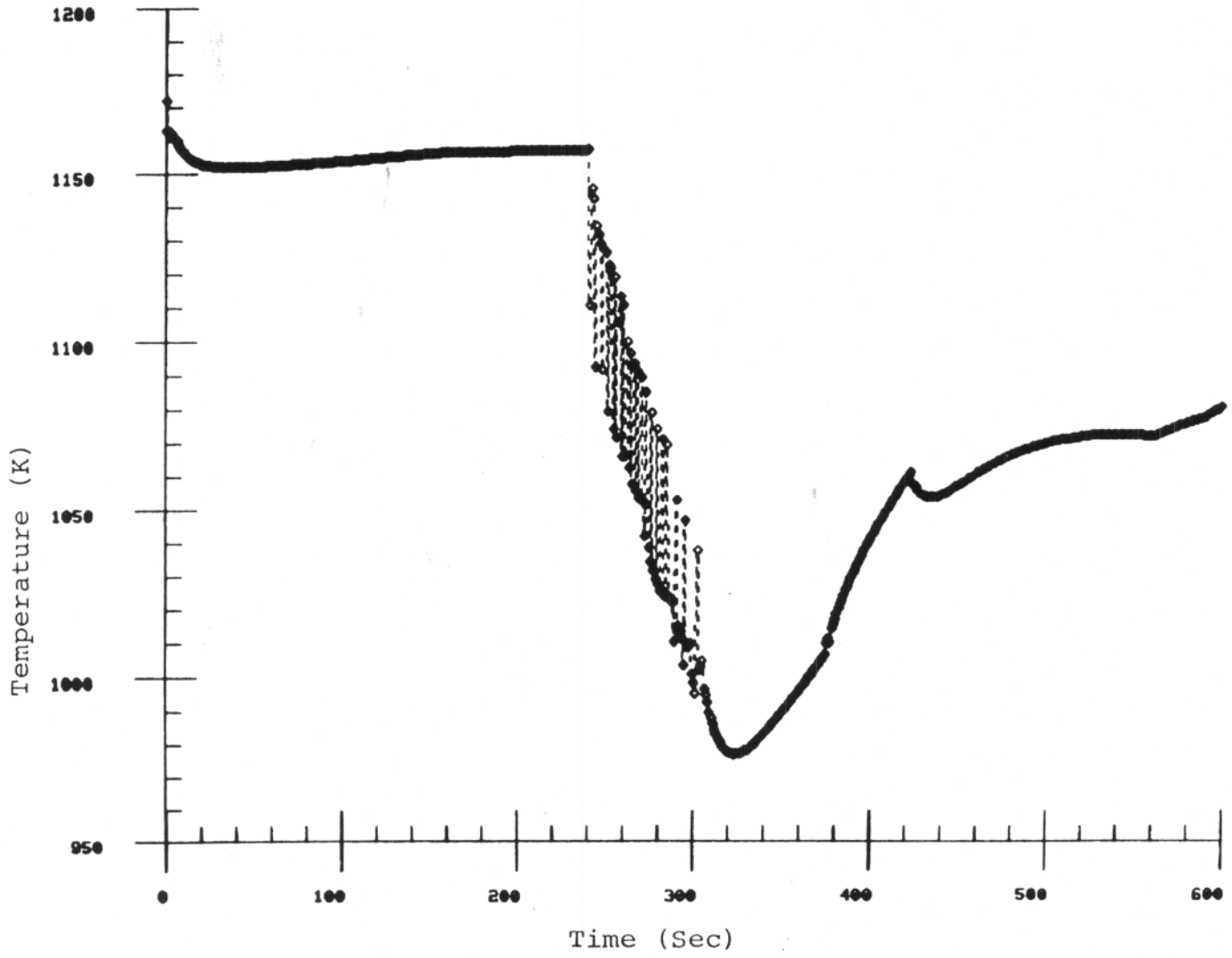

Figure 30. Flame Temperature.

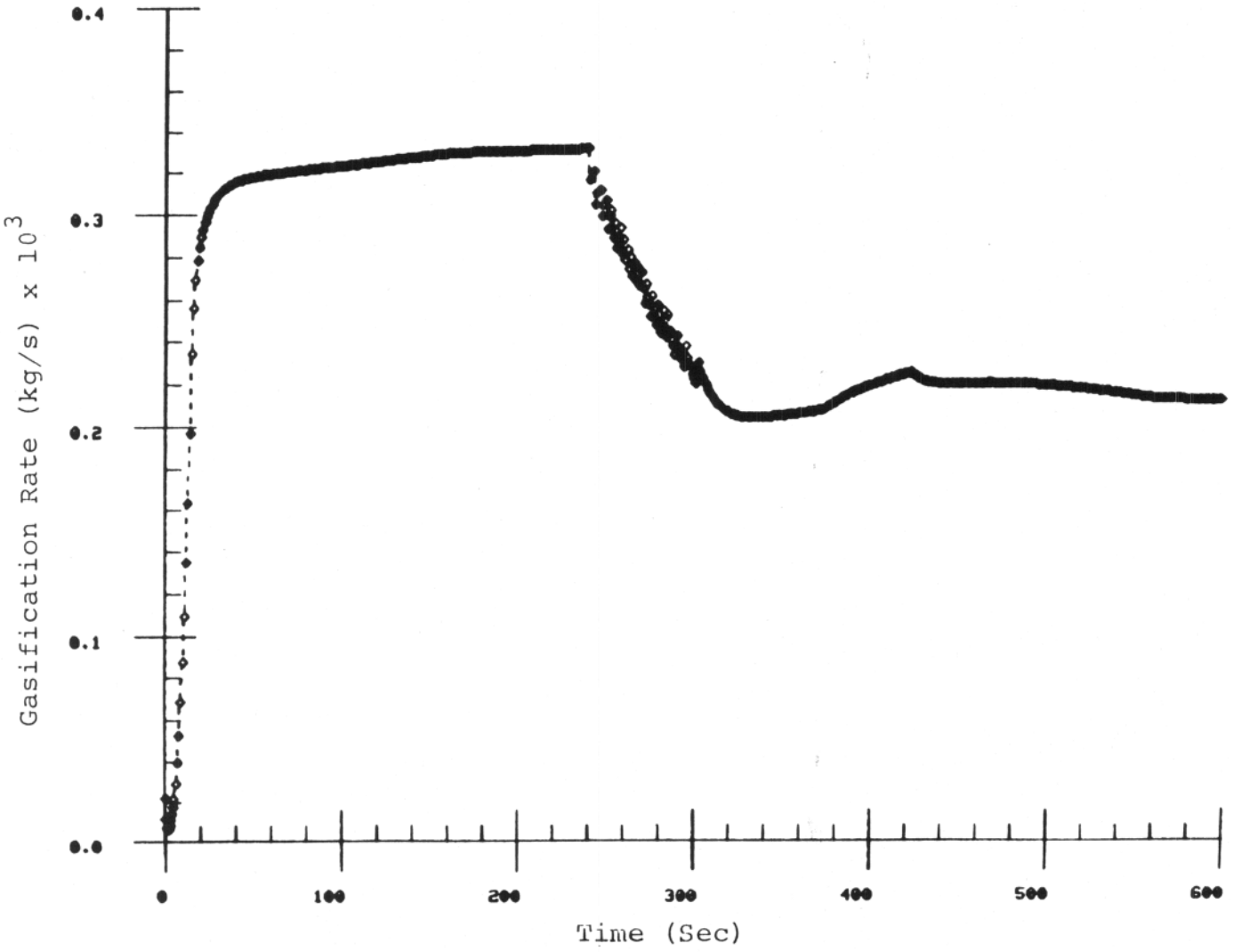

Figure 31. Fuel Gasification Rate.

constant value of 0.21 x 10^{-3} kg/s (0.46x10^{-3}lbm/s). By the end of the run, the rate seems to be very slowly decreasing.

In many of the figures above, we note that for the very first few seconds of the simulation the values of quantitites such as the flame height and mass burning rate oscillate for a few steps before a definite trend is established. This is due to the fact that we must estimate an initial burning rate at the start (in the input) and this estimate may not be exactly in agreement with the value computed for the flame radiation at the end of the first integration step. Therefore, it takes a few steps for the program to find a compatible set of flame height, flame heat transfer, and burning rate values. Also during this time, the prescribed change in the fire base radius from 0.01 meters to 0.182 meters by 15 seconds is taking place. This increase in the fire size can be seen in the mass burning rate and flame height curves which, after the initial oscillation to establish the correct burning rate, rise quickly and then attain steady values after 15 seconds.

The general conclusions that we may draw from the sample case are that for this particular volume and ventilation rate, the polyurethane foam fire will be able to maintain a vigorous burning throughout the 10 minutes of the run. The burning rate does decrease by approximately one-third as the flames move into the combustion products of the hot zone, but the fire is nowhere near extinction. The influence of the increased radiation from the hot zone offsets the influence of the decreased absorption coefficient and flame temperature so that the burning rate is approximately constant or only very slightly declining at 10 minutes. The temperature of the hot zone is only about 30 K (54°F) above the starting temperature, so that we certainly should expect the materials of the walls and the ceilings to be unaffected by the fire to this point; with, perhaps, the exception of a local

hot spot at the plume impingement point. The interior pressure rise is negligible and, indeed, after a transient period, returns to the value that was set in the input.

While the current version of the CCFM does not monitor the amount of fuel consumed directly, we can obtain this number from an integration of the mass burning rate shown in Figure 31 over the 600 seconds. When this is done, we find that during the 10 minute period, about 0.16 kg of the polyurethane foam has been consumed. Assuming that the foam has a density of 16 kg per cubic meter (1 pound per cubic foot) this means that about 0.01 cubic meters (0.35 cubic feet) burns in this time, and this is consistent with the observation that this fire would not be likely to break out of the compartment.

SECTION 4
SUMMARY AND CONCLUSIONS

In summary, we have constructed a zone model of fire within the cargo compartment which incorporates the effect of oxygen consumption on the fire development. The model assumes that the primary effect of the progressively lowering oxygen concentration is the reduction of the feedback of heat from the fire flames to the fuel surface. As the concentration lowers, the flame temperature and emittance are reduced and so the rate of fuel vaporization declines. The process accelerates as the hot zone moves down over the flame.

While we expect this model to have incorporated most of the significant processes involved, we have ignored, for lack of applicable theory, such phenomena as the ultimate extinction limit for fires of this type. We have also taken a very simple model of the fuel reaction to the input heat from the flame: that of assuming pure substance vaporization. And lastly, we have not considered the growth of the base area which can be expected to occur in most real fuel arrays.

Notwithstanding these possible deficiencies, solutions for sample cases run to date show what appears to be physically realistic behavior. Until the results of validation experiments are available and a comparison to the model is made, we can only speculate as to what improvements will be needed, if any, to the CCFM. It is most likely that some method of incorporating fire spread will be necessary. Almost any fire in a loaded compartment should spread to some extent before oxygen depletion effects come into play. Further work will also be required in determining the fire behavior as the oxygen concentration drops to low levels, approximately less than 0.16 or 0.15 mass fraction. We think that chemical kinetic factors may serve to further lower

the burning rate or even cause active flaming to cease completely.

Although it does not seem to have a significant effect on the overall solution, the oscillating flame height, which occurs as the hot zone interface moves over the flame tip, is definitely a model deficiency. Our attempt to remove this oscillation was to arbitrarily damp the flame height change by averaging over a three second interval. This time interval was chosen arbitrarily but should be larger than most turbulent fluctuations in a real fire. While this reduced the oscillations to a great degree, it did not completely eliminate them, and we still see their effect in small oscillations in the mass burning rate. Different approaches should be investigated to stabilize the burning rate when the flame tip reaches the hot zone.

Another factor which we suspect will become apparent in validation experiments is a deviation from the idealized two zone division of the compartment atmosphere. Ventilation may force some mixing of the combustion products into what we regard as the cool zone, reducing its oxygen concentration and perhaps raising its temperature and combustion product concentration to a non-negligible amount. Simple models can be proposed for this process, but any interzone mixing model would have to be primarily empirical in nature, containing adjustable constants or functions determined from experiment.

Another factor not incorporated in the model is the effect of the load thermal mass and volume. When the load takes up a large part of the interior volume, it will obviously have a significant effect upon the rate of filling by the hot zone gas and the heat exchange between the gases and the interior surfaces. Because the shape and distribution of the load are not easy to specify, it may be necessary to take a semi-statistical approach to describing the load. Such a statistical description might

employ a function which gives the average surface contact area and average volume of the load as a function of height above the floor. These average values should be then incorporated in the governing equations in those places where the zone volume and the convective heat transfer appear.

The Gauss-Seidel numerical technique for solving the governing equation seems to be reasonably robust, but not as efficient as we should want. There are occasions where the program requires a excessive amount of time between solutions, and this is particularly inconvenient for interactive use. Further work is needed in improving the efficiency of the numerical procedure.

SECTION 5

REFERENCES

1. MacArthur, C. D., "Dayton Aircraft Cabin Fire Model, Version 3, Volume 1 - Physical Description," DOT/FAA/CT-81/69-1, June 1982.

2. Emmons, H. W., "The Prediction of Fires in Buildings," Seventeenth Symposium (International) on Combustion, The Combustion Institute, 1978, pp. 1101-1111.

3. Quintiere, J. G. and B. J. McCaffrey, "The Burning of Wood and Plastic Cribs in an Enclosure: Volume 1," NBSIR 80-2054, November 1980.

4. Mitler, H. E., "The Physical Basis for the Harvard Computer Fire Code," Home Fire Project Technical Report No. 34, Harvard University, October 1978.

5. Seigel, R. and J. R. Howell, Thermal Radiation Heat Transfer, McGraw-Hill Book Company, New York, 1972.

6. Mitler, H. E. and H. W. Emmons, "Documentation for CFC V, the Fifth Harvard Computer Fire Code," NBS-GCR-81-344, October 1981.

7. Hottel, H. C., and Sarofim, A. F., Radiative Transfer, McGraw-Hill Book Company, New York, 1967.

8. Modak, A. T., "Radiation from Products of Combustion," FMRC Technical REport RC78-BT-28, Octoaber 1978.

9. Steward, F. R., "Prediction of the Height of Turbulent Diffusion Buoyant Flames," Combustion Science and Technology, Volume 2, (1970), pp. 203-212.

10. deRis, J., "A Stochastic Combustion Model for Fire Plumes," Fire Safety Journal, Vol. 5, No. 2, (1981).

11. Tamanini, F., "Reaction Rates, Air Entrainment and Radiation in Turbulent Fire Plumes," Combustion and Flame, Vol. 30, (1977), pp. 85-101.

12. deRis, J., "Fire Radiation - A Review," Seventeenth Symposium (International) on Combustion, The Combustion Institute, 1979, pp. 1003-16

13. McCaffrey, B. J., "Purely Buoyant Diffusion Flames: Some Experimental Results," NBSIR 79-1910, October, 1979.

14. Santo, G., "Influence of Oxygen Depletion on the Radiative Properties of PMMA Flames," Factory Mutual Research Corporation Report, J.I. 0A0E6.Bu-3, August 1979.

15. Cooper, L. Y., "Heat Transfer from a Buoyant Plume to an Unconfined Ceiling," Paper 81-HT-7 preseented at the 20th ASME/AICHE Heat Transfer Conference, Milwaukee, WI, August 1981.

16. Kays, W. M., and M. E. Crawford, Convective Heat and Mass Transfer. 2nd ed., McGraw-Hill, New York, 1980.

17. Kreith, F., Principles of Heat Transfer, 3rd ed., Intext Educational Publishers, New York, 1973.

18. Tewarson, A., "Physico-Chemical and Combustion/Pyrolysis Properties of Polymeric Materials," NBS-GCR-80-295, December, 1980.

19. Weast, R. C., Editor, Handbook of Chemistry and Physics, 51st ed., The Chemical Rubber Co., Cleveland, OH, 1971.

APPENDIX A

A.1 THE COOL ZONE THICKNESS

The cool zone thickness computation assumes that the cargo compartment's cross section (shape) has been approximated by a closed, convex polygon in the x-z plane, and that this cross section is uniform for the entire compartment length. In addition, the force of gravity is assumed to be in the negative z direction. First, the cool zone's true cross-sectional area is computed by dividing the current cool zone volume by the compartment's length. Then, using the previous thickness as an initial estimate, the cool zone thickness is modified until it is consistent with the true cross-sectional area of the cool zone.

Each estimate of the cool zone thickness defines a cool zone cross section that can be represented by a convex polygon in the x-z plane. The area of this polygon can be computed using the following equation: *

$$A = (1/2) \left| \sum_{i=1}^{N-1} (x_i z_{i+1} - x_{i+1} z_i) \right|$$

where A = area of polygon,

N = total number of points used to describe the polygon,

x_i = x coordinate of i^{th} point describing the polygon,

and z_i = z coordinate of the i^{th} point describing the polygon.

The cool zone thickness is then adjusted (based on the relative difference between the areas) until the cross-sectional area computed from the thickness estimate is the same as the true cross-sectional area of the cool zone (within a specified tolerance).

---

* MacArthur, Charles D. and Jerry B. Reeves, "Aircraft Ground Fire Suppression and Rescue Simulation Model" Appendix A.

A.2 COEFFICIENTS FOR EQUATION (34)

Equation (34) provides the following analytic approximation for the solution of the integral $I(\beta)$:

$$I(\beta) = \int_{\gamma}^{2.7} [\psi - \gamma] \exp\left[-\sum_{n=0}^{6} a_n \psi^n\right] d\psi = \begin{cases} \exp\left(-c_e \gamma^2\right) & , \gamma \geq 1.68 \\ \sum_{i=0}^{4} c_i \gamma^i & , \gamma < 1.68 \end{cases}$$

where $\gamma = r_c \beta / (1 + r_c)$

$c_e = 1.59861$

$c_0 = 0.995151$

$c_1 = -0.840780$

$c_2 = -0.244122$

$c_3 = 0.379948$

$c_4 = -0.0858938$

$a_0 = 1.7573$

$a_1 = -0.46139$

$a_2 = -1.2214$

$a_3 = -1.5843$

$a_4 = 2.3693$

$a_5 = -0.62914$

$a_6 = 0.026405$

A.3 ENTRAINMENT EXPRESSION FOR THE FIRE MODEL

The following fourth-degree polynomial is used to approximate the fire's entrainment coefficient in the CCFM model:

$$K(\alpha) = \sum_{i=0}^{4} c_i Y_f^{\,i}$$

where $Y_f = Y_{fo}(1 + r_c)\, I(\alpha)/\alpha$ = fuel mass fraction inside the plume

$c_0 = 0.531031$

$c_1 = -0.457271$

$c_2 = 0.603383$

$c_3 = 0.356424$

$c_4 = -0.878467$

A.4 FLAME/PLUME TEMPERATURE COMPUTATION

An iterative procedure is used to compute the flame/plume temperature at a specific location inside the fire. First, an initial estimate of the specific heat of the plume gas is computed by solving the following equation with T = 1200°K.

$$c_p(T) = a_0 + a_1(\theta^{-1.5}) + a_2(\theta^{-2}) + a_3(\theta^{-3})$$

where T = plume temperature estimate (°K)

θ = T/100

a_0 = 1394

a_1 = -18310

a_2 = 38293

a_3 = -29290

This specific heat estimate is then substituted into equation (39) to obtain a new flame/plume temperature estimate. Each new temperature estimate is used to compute a new specific heat estimate until the relative difference between two successive temperature estimates is less than 1%.

A.5 INTEGRAL APPROXIMATION FOR EQUATIONS (47) AND (53)

Equations (47) and (53) provide expressions for the oxygen mass fraction inside the plume at the zone interface and the compartment ceiling, respectively. The integral appearing in both expressions can be approximated by a fourth degree polynomial as follows:

$$\int_0^{\gamma} [\gamma - \psi] \exp\left[-\sum_{n=0}^{6} a_n \psi^n\right] d\psi = \sum_{i=0}^{4} c_i \gamma^i$$

where $\gamma = r_h \eta_c/(1 + r_h)$ or $\gamma = r_c \zeta_i/(1+r_c)$

c_0 = 0.0024063

c_1 = 0.00583727

c_2 = -0.0436571

$c_3 = 0.228826$

$c_4 = -0.0507843$

The a_n coefficients in the above expression are identical to those listed in section A.2.